ELSEVIER

Composites: Part A 32 (2001) 143–172

composites
Part A: applied science and manufacturing

www.elsevier.com/locate/compositesa

Simulation of the mechanical properties of fibrous composites by the bridging micromechanics model

Zheng-Ming Huang*

Department of Mechanics, Huazhong University of Science & Technology, Wuhan, Hubei 430074, People's Republic of China

Received 27 September 1999; revised 27 July 2000; accepted 15 August 2000

Abstract

The overall thermal–mechanical properties of a fibrous composite out of an elastic deformation range can be simply simulated using a recently developed micromechanics model, the Bridging Model. Only the in situ constituent fiber and matrix properties of the composite and the fiber volume fraction are required in the simulation. This general yet easy-to-implement micromechanics model is reviewed and summarized in the present paper. Application of the model to predict various properties of unidirectional laminae and multidirectional laminates, including thermoelastic behavior, elasto-plastic response, ultimate failure strength, strength at elevated temperature, and fatigue strength and $S–N$ curve, is demonstrated. It is suggested that use of the bridging model, appropriately calibrated with experimental data, can therefore inform composite design by identifying suitable constituent materials, their contents, and their geometrical arrangements. Some technical issues regarding applications of the bridging model are also addressed.

Keywords: A. Fibres; A. Laminates; A. Metal-matrix composites (MMCs); B. Mechanical properties

1. Introduction

Over the last four decades or so, a great number of micromechanics models have been proposed in the literature. Surveys about these models can be found, among others, in Refs. [1–5]. Most these models can be used to accurately estimate the linear elastic property of a fibrous composite. However, it is difficult to generalize them to the inelastic deformation situations. The majority of these models, without significant modifications, cannot be applied to predict the yield strength, failure strength, or the nonlinear stress–strain relationship of fibrous composites, since the existing models for estimating composite elastic behavior do not have any inherent connections with the other mechanical properties of the composites.

Yet, several attempts have been made to understand micromechanically the inelastic and failure behaviors of composites by using their constituent properties and geometric parameters [6]. One such model is the concentric cylinder model [7], well known in analyzing lamina elastic properties [2,3]. A concentric cylinder representative volume element (see Fig. A1) is taken for the composite, and a set of governing equations on this geometry are solved using, e.g. Finite Difference method. However, it is difficult to use this model to simulate the composite responses under transverse and in-plane shear loads, and hence the model cannot perform general composite laminate analysis. Dvorak and Bahei-El-Din [8,9] developed a vanishing fiber diameter model. This model assumes that the fibers possess a vanishingly small diameter even though they occupy a finite volume fraction of the composite. Only the longitudinal constraints between the fibers and the matrix have been considered in the model. Rule of mixtures assumptions have been made for the averaged stress and strain relations. Therefore, the model gives exactly the same predictions as the rule-of-mixtures formulae for composite elastic properties. As we know, these predictions are not accurate for the composite transverse and in-plane shear responses. Hopkins and Chamis [10,11] proposed a multicell model, by requiring that longitudinal strains and transverse stresses in the fiber and matrix be equal to each other. This is similar to the rule of mixture assumption. The material nonlinearity is described as a multifactor interaction relationship, whereas each material property is described as a product of many power law equations each of which indicates how that property is affected by one parameter. Aboudi [12,13] developed a method of cells

* Present address: Materials Science Division, Department of Mechanical & Production Engineering, National University of Singapore, 10 Kent Ridge Crescent, Singapore 119260. E-mail: mpehzm@ nus.edu.sg.

E-mail address: huangzm@email.com (Z.-M. Huang).

1359-835X/01/$ - see front matter
PII: S1359-835X(00)00142-1

model in a rather general sense. The main drawback of this model is in its complexity. In fact, Teply and Reddy [14] have shown that the method of cells model can be reformulated and cast in the form of a finite element analysis by employing the Hellinger–Reissner variational principle. The user-unfriendly feature of this model is thus clearly seen. Further, a regular fiber packing pattern must be preassumed before applying the method of cells model. As has been investigated by Brockenbrough et al. [15], the composite transverse and in-plane shear responses at a plastic region are sensitive to the fiber packing patterns assumed. They found that predictions for the transverse and in-plane shear responses based on any of their regular fiber packing patterns do not correlate well with experiments. It is seen that a significant advancement on micromechanical simulation of composite inelastic and failure properties is necessary.

Recently, the author developed a new versatile and user-friendly micromechanics model, named as the Bridging Model. The key step of the model is to correlate the averaged stress states in the constituent fiber and matrix by using a bridging matrix. As the bridging matrix can only depend on the constituent properties and on the fiber packing geometry in the matrix (Appendix B), a unified model is established by focusing on determination of the bridging matrix for composite elastic responses. This is achieved by making use of some established elastic solutions for composites in the literature. An extension of the so-defined bridging matrix to an inelastic region is straightforward: only the constituent properties involved need to be changed because the fiber packing geometry does not change or only varies to a negligibly small amount when the constituents undergo inelastic deformation. The bridging model can be applied to predict the effective properties of a unidirectional (UD) composite made from any constituent fiber and matrix materials [16–19,21–23]. These properties include the thermo-elastic constants, yield strength, failure strength, ultimate strain, rubber–elastic stress–strain curve, etc. The prediction only uses the in situ constituent properties and the fiber volume fraction. In the case where the fibers are linearly elastic until rupture and the matrix is bilinearly elastic–plastic, closed-form formulae for composite strengths under uniaxial loads (longitudinal tension, transverse tension, and in-plane shear) are obtainable [24,25], which are as concise as the rule of mixtures formulae for composite stiffness. The bridging model has been successfully applied to simulate inelastic and failure behaviors of composite laminates [20,26–29], fatigue properties and *S–N* data of fibrous laminae and laminates [30,31], and elastic, inelastic and strength responses of various textile (woven, braided, and knitted) fabric reinforced composites subjected to in-plane as well as flexural loads [32–43]. The purpose of this paper is to summarize and review the bridging model developed as well as its potential applications to unidirectional laminae and multidirectional laminates.

2. The bridging micromechanics model

2.1. Model development [16,21–23]

Consider a UD fibrous composite. Casting in an incremental form, the volume averaged stress increments in the fibers and matrix of the composite can be correlated using a bridging matrix through

$$\{\mathrm{d}\sigma_i^{\mathrm{m}}\} = [A_{ij}]\{\mathrm{d}\sigma_j^{\mathrm{f}}\} \tag{1}$$

where $\{\mathrm{d}\sigma_i\} = \{\mathrm{d}\sigma_{11}, \mathrm{d}\sigma_{22}, \mathrm{d}\sigma_{33}, \mathrm{d}\sigma_{23}, \mathrm{d}\sigma_{13}, \mathrm{d}\sigma_{12}\}^{\mathrm{T}}$ and the suffixes "f" and "m" refer to the fiber and matrix, respectively. A quantity without any suffix in the following will refer to the composite. The bridging matrix $[A_{ij}]$ represents the load share capacity of one constituent phase (the fiber or the matrix) in the composite with respect to the other phase (the matrix or the fiber). Substituting Eq. (1) into the volume averaged stress relationship (see Appendix A)

$$\{\mathrm{d}\sigma_i\} = V_{\mathrm{f}}\{\mathrm{d}\sigma_i^{\mathrm{f}}\} + V_{\mathrm{m}}\{\mathrm{d}\sigma_i^{\mathrm{m}}\}, \tag{2a}$$

and making use of (Appendix A)

$$\{\mathrm{d}\varepsilon_i\} = V_{\mathrm{f}}\{\mathrm{d}\varepsilon_i^{\mathrm{f}}\} + V_{\mathrm{m}}\{\mathrm{d}\varepsilon_i^{\mathrm{m}}\}, \tag{2b}$$

$$\{\mathrm{d}\varepsilon_i^{\mathrm{f}}\} = [S_{ij}^{\mathrm{f}}]\{\mathrm{d}\sigma_j^{\mathrm{f}}\}, \tag{2c}$$

$$\{\mathrm{d}\varepsilon_i^{\mathrm{m}}\} = [S_{ij}^{\mathrm{m}}]\{\mathrm{d}\sigma_j^{\mathrm{m}}\}, \tag{2d}$$

$$\{\mathrm{d}\varepsilon_i\} = [S_{ij}]\{\mathrm{d}\sigma_j\}, \tag{2e}$$

the overall instantaneous compliance matrix of the composite as well as the stress increments shared by the fiber and matrix are derived, respectively, as (Appendix B)

$$[S_{ij}] = (V_{\mathrm{f}}[S_{ij}^{\mathrm{f}}] + V_{\mathrm{m}}[S_{ij}^{\mathrm{m}}][A_{ij}])(V_{\mathrm{f}}[I] + V_{\mathrm{m}}[A_{ij}])^{-1}, \tag{3}$$

$$\{\mathrm{d}\sigma_i^{\mathrm{f}}\} = (V_{\mathrm{f}}[I] + V_{\mathrm{m}}[A_{ij}])^{-1}\{\mathrm{d}\sigma_j\} = [B_{ij}]\{\mathrm{d}\sigma_j\}, \tag{4a}$$

$$\{\mathrm{d}\sigma_i^{\mathrm{m}}\} = [A_{ij}](V_{\mathrm{f}}[I] + V_{\mathrm{m}}[A_{ij}])^{-1}\{\mathrm{d}\sigma_j\} = [A_{ij}][B_{ij}]\{\mathrm{d}\sigma_j\}. \tag{4b}$$

In the above, V denotes the volume fraction, $\{\mathrm{d}\varepsilon_j\} = \{\mathrm{d}\varepsilon_{11}, \mathrm{d}\varepsilon_{22}, \mathrm{d}\varepsilon_{33}, 2\mathrm{d}\varepsilon_{23}, 2\mathrm{d}\varepsilon_{13}, 2\mathrm{d}\varepsilon_{12}\}^{\mathrm{T}}$, and $[I]$ is a unit matrix. In practice, the fibers used are generally at most transversely isotropic and the matrix is isotropic. The resulting UD composite is then considered as transversely isotropic. There are only five independent elements in $[S_{ij}]$, and so are in $[A_{ij}]$. Further, $[S_{ij}]$ must be symmetric, i.e.

$$S_{ij} = S_{ji}, \qquad i,j = 1,2,\ldots,6. \tag{5}$$

Therefore, the bridging matrix, $[A_{ij}]$, has the general form

[16,17,21,22] (also see Appendix B)

$$[A_{ij}] = \begin{bmatrix} a_{11} & a_{12} & a_{13} & a_{14} & a_{15} & a_{16} \\ 0 & a_{22} & a_{23} & a_{24} & a_{25} & a_{26} \\ 0 & a_{32} & a_{33} & a_{34} & a_{35} & a_{36} \\ 0 & 0 & 0 & a_{44} & a_{45} & a_{46} \\ 0 & 0 & 0 & 0 & a_{55} & a_{56} \\ 0 & 0 & 0 & 0 & 0 & a_{66} \end{bmatrix}. \tag{6}$$

In the above, a_{11}, a_{22}, a_{33}, a_{66}, and a_{32} are independent elements. $a_{55} = a_{66}$ due to the fact that shear stress–strain responses in (1,2) and (1,3) planes are the same, whereas a_{44} is not independent because of a correlation among the transverse Young's modulus, shear modulus, and transverse Poisson's ratio (see Eq. (B7)). The remaining 15 nonzero elements are determined from Eq. (5) together with Eq. (3).

For simplicity, let the fiber become isotropic in a plastic region. Such typical fibers are glass, carbon/graphite, aramid, boron, silicon carbide, alumina, etc. which can be considered as linearly elastic until rupture. Further, suppose that the matrix is an elastic–plastic material. When the matrix undergoes a rubber–elastic deformation, Ref. [19] provided an approach methodology, see also Refs. [37,38]. With these assumptions, the independent bridging elements in (6) are given by [16,17,21,22] (see also Appendix B)

$$a_{11} = E_{\mathrm{m}}/E_{\mathrm{f1}}, \tag{7a}$$

$$a_{22} = a_{33} = a_{44} = \beta + (1-\beta)\frac{E_{\mathrm{m}}}{E_{\mathrm{f2}}}, \tag{7b}$$

$0 < \beta < 1$ ($\beta = 0.35$–0.5 in most cases),

$$a_{55} = a_{66} = \alpha + (1-\alpha)\frac{G_{\mathrm{m}}}{G_{\mathrm{f}}}, \tag{7c}$$

$0 < \alpha < 1$ ($\alpha = 0.3$–0.5 in most cases),

$$a_{32} = 0. \tag{7d}$$

It should be noted that since the independent element a_{32} also takes zero, the bridging matrix is simply given by an upper triangle, as given in Ref. [22]. In the above, E_{m}, G_{m}, E_{f1}, E_{f2}, and G_{f} are called effective moduli and are defined as

$$E_{\mathrm{m}} = \begin{cases} E^{\mathrm{m}}, & \text{when } \sigma_{\mathrm{e}}^{\mathrm{m}} \le \sigma_{\mathrm{Y}}^{\mathrm{m}} \\ E_{\mathrm{T}}^{\mathrm{m}}, & \text{when } \sigma_{\mathrm{e}}^{\mathrm{m}} > \sigma_{\mathrm{Y}}^{\mathrm{m}} \end{cases} \tag{8a}$$

$$G_{\mathrm{m}} = \begin{cases} 0.5E^{\mathrm{m}}/(1+\nu^{\mathrm{m}}), & \text{when } \sigma_{\mathrm{e}}^{\mathrm{m}} \le \sigma_{\mathrm{Y}}^{\mathrm{m}} \\ E_{\mathrm{T}}^{\mathrm{m}}/3, & \text{when } \sigma_{\mathrm{e}}^{\mathrm{m}} > \sigma_{\mathrm{Y}}^{\mathrm{m}} \end{cases} \tag{8b}$$

$$E_{\mathrm{f1}} = \begin{cases} E_{11}^{\mathrm{f}}, & \text{when } \sigma_{\mathrm{e}}^{\mathrm{f}} \le \sigma_{\mathrm{Y}}^{\mathrm{f}} \\ E_{\mathrm{T}}^{\mathrm{f}}, & \text{when } \sigma_{\mathrm{e}}^{\mathrm{f}} > \sigma_{\mathrm{Y}}^{\mathrm{f}} \end{cases} \tag{8c}$$

$$E_{\mathrm{f2}} = \begin{cases} E_{22}^{\mathrm{f}}, & \text{when } \sigma_{\mathrm{e}}^{\mathrm{f}} \le \sigma_{\mathrm{Y}}^{\mathrm{f}} \\ E_{\mathrm{T}}^{\mathrm{f}}, & \text{when } \sigma_{\mathrm{e}}^{\mathrm{f}} > \sigma_{\mathrm{Y}}^{\mathrm{f}} \end{cases} \tag{8d}$$

$$G_{\mathrm{f}} = \begin{cases} G_{12}^{\mathrm{f}}, & \text{when } \sigma_{\mathrm{e}}^{\mathrm{f}} \le \sigma_{\mathrm{Y}}^{\mathrm{f}} \\ E_{\mathrm{T}}^{\mathrm{f}}/3, & \text{when } \sigma_{\mathrm{e}}^{\mathrm{f}} > \sigma_{\mathrm{Y}}^{\mathrm{f}} \end{cases} \tag{8e}$$

E^{m}, ν^{m}, and $E_{\mathrm{T}}^{\mathrm{m}}$ are Young's modulus, Poisson's ratio, and hardening modulus (tangent to the uniaxial stress–strain curve in a plastic region) of the matrix, respectively. E_{11}^{f}, E_{22}^{f}, G_{12}^{f}, and $E_{\mathrm{T}}^{\mathrm{f}}$ are the longitudinal, transverse, in-plane shear, and hardening moduli of the fibers, respectively. σ_{Y} represents the yield strength of a material (fibers or matrix), whereas σ_{e} is the von Mises effective stress of the material defined using three principal stresses of the material, σ^1, σ^2, and σ^3 ($\sigma^1 \ge \sigma^2 \ge \sigma^3$), via

$$\sigma_{\mathrm{e}} = \sqrt{\tfrac{1}{2}[(\sigma^1-\sigma^2)^2 + (\sigma^2-\sigma^3)^2 + (\sigma^3-\sigma^1)^2]}. \tag{9}$$

2.2. Elastic response [16,21,22]

When both the fibers and the matrix are in elastic deformation, all the dependent elements of the bridging matrix, Eq. (6), are zero except for a_{12} and a_{13}, which read

$$a_{13} = a_{12} = (S_{12}^{\mathrm{f}} - S_{12}^{\mathrm{m}})(a_{11} - a_{22})/(S_{11}^{\mathrm{f}} - S_{11}^{\mathrm{m}}). \tag{10}$$

Hence, the five engineering moduli of the composites are found to be (Appendix B)

$$E_{11} = V_{\mathrm{f}}E_{11}^{\mathrm{f}} + V_{\mathrm{m}}E^{\mathrm{m}}, \tag{11a}$$

$$\nu_{12} = V_{\mathrm{f}}\nu_{12}^{\mathrm{f}} + V_{\mathrm{m}}\nu^{\mathrm{m}}, \tag{11b}$$

$$E_{22} = \frac{(V_{\mathrm{f}} + V_{\mathrm{m}}a_{11})(V_{\mathrm{f}} + V_{\mathrm{m}}a_{22})}{(V_{\mathrm{f}} + V_{\mathrm{m}}a_{11})(V_{\mathrm{f}}S_{22}^{\mathrm{f}} + a_{22}V_{\mathrm{m}}S_{22}^{\mathrm{m}}) + V_{\mathrm{f}}V_{\mathrm{m}}(S_{21}^{\mathrm{m}} - S_{21}^{\mathrm{f}})a_{12}}, \tag{11c}$$

$$G_{12} = \frac{(V_{\mathrm{f}} + V_{\mathrm{m}}a_{66})G_{12}^{\mathrm{f}}G^{\mathrm{m}}}{V_{\mathrm{f}}G^{\mathrm{m}} + V_{\mathrm{m}}a_{66}G_{12}^{\mathrm{f}}}, \tag{11d}$$

$$G_{23} = \frac{0.5(V_{\mathrm{f}} + V_{\mathrm{m}}a_{44})}{V_{\mathrm{f}}(S_{22}^{\mathrm{f}} - S_{23}^{\mathrm{f}}) + V_{\mathrm{m}}a_{44}(S_{22}^{\mathrm{m}} - S_{23}^{\mathrm{m}})}. \tag{11e}$$

It is noted that Eqs. (11a) and (11b) are obtained based on bridging element formulae (7a) and (7d), whereas Eqs. (11c)–(11e) are based on formulae (7b) and (7c).

2.3. Plastic response [17,21,22]

As long as any constituent has undergone a plastic deformation, the composite is defined to have such a deformation too. In such case, only the instantaneous compliance matrix of the constituent, $[S_{ij}^{\mathrm{f}}]$ or $[S_{ij}^{\mathrm{m}}]$, needs to be redefined. It is to be noted that the fibers have been assumed to take isotropic hardening. Hence, both the constituent materials can use a same plastic flow theory to define their instantaneous compliance matrices. Many such theories have been

developed, and any of them can be equally well incorporated with the bridging model. Let the general Prandtl–Reuss theory be employed, which gives [22,44]

$$[S_{ij}] = \begin{cases} [S_{ij}]^{\mathrm{e}}, & \text{when } \tau_0 \le \dfrac{\sqrt{2}}{3}\sigma_{\mathrm{Y}} \\ [S_{ij}]^{\mathrm{e}} + [S_{ij}]^{\mathrm{p}}, & \text{when } \tau_0 > \dfrac{\sqrt{2}}{3}\sigma_{\mathrm{Y}} \end{cases} \tag{12}$$

$$\tau_0 = \left[\frac{1}{3}\sigma'_{ij}\sigma'_{ij}\right]^{1/2}, \tag{13}$$

$$\sigma'_{ij} = \sigma_{ij} - \frac{1}{3}\sigma_{kk}\delta_{ij}. \tag{14}$$

In Eqs. (13) and (14), a summation is applied to the repeated suffixes, and σ_{ij} are total stresses. In Eq. (12), $[S_{ij}]^{\mathrm{e}}$ is the elastic component of the compliance matrix specified by Hooke's law, and $[S_{ij}]^{\mathrm{p}}$ is the plastic component defined as [22,44]

$$[S_{ij}]^{\mathrm{p}} = \frac{1}{2M_{\mathrm{T}}(\tau_0)^2} \times \begin{bmatrix} \sigma'_{11}\sigma'_{11} & \sigma'_{22}\sigma'_{11} & \sigma'_{33}\sigma'_{11} & 2\sigma'_{23}\sigma'_{11} & 2\sigma'_{13}\sigma'_{11} & 2\sigma'_{12}\sigma'_{11} \\ & \sigma'_{22}\sigma'_{22} & \sigma'_{33}\sigma'_{22} & 2\sigma'_{23}\sigma'_{22} & 2\sigma'_{13}\sigma'_{22} & 2\sigma'_{12}\sigma'_{22} \\ & & \sigma'_{33}\sigma'_{33} & 2\sigma'_{23}\sigma'_{33} & 2\sigma'_{13}\sigma'_{33} & 2\sigma'_{12}\sigma'_{33} \\ & & & 4\sigma'_{23}\sigma'_{23} & 4\sigma'_{13}\sigma'_{23} & 4\sigma'_{12}\sigma'_{23} \\ & & & & 4\sigma'_{13}\sigma'_{13} & 4\sigma'_{12}\sigma'_{13} \\ \text{symmetry} & & & & & 4\sigma'_{12}\sigma'_{12} \end{bmatrix}, \tag{15}$$

$$M_{\mathrm{T}} = \frac{E_{11}E_{\mathrm{T}}}{E_{11} - E_{\mathrm{T}}}. \tag{16}$$

Note that for the matrix material, $E_{11} = E$. Note also that the plastic component, $[S_{ij}]^{\mathrm{p}}$, can only occur in a loading condition. Whenever there is an unloading, the compliance matrix is simply given by its elastic component.

2.4. Planar formulae [23]

If the composite is only subjected to a planar load, as it generally is in practice, the stress states in the constituents are correlated through

$$\begin{Bmatrix} \mathrm{d}\sigma^{\mathrm{m}}_{11} \\ \mathrm{d}\sigma^{\mathrm{m}}_{22} \\ \mathrm{d}\sigma^{\mathrm{m}}_{12} \end{Bmatrix} = \begin{bmatrix} a_{11} & a_{12} & a_{16} \\ 0 & a_{22} & a_{26} \\ 0 & 0 & a_{66} \end{bmatrix} \begin{Bmatrix} \mathrm{d}\sigma^{\mathrm{f}}_{11} \\ \mathrm{d}\sigma^{\mathrm{f}}_{22} \\ \mathrm{d}\sigma^{\mathrm{f}}_{12} \end{Bmatrix}. \tag{17}$$

In Eq. (17), a_{12} is defined by Eq. (10), and the other off-diagonal elements are given by

$$a_{16} = \frac{d_2\beta_{11} - d_1\beta_{21}}{\beta_{11}\beta_{22} - \beta_{12}\beta_{21}}, \tag{18a}$$

$$a_{26} = \frac{d_1\beta_{22} - d_2\beta_{12}}{\beta_{11}\beta_{22} - \beta_{12}\beta_{21}}, \tag{18b}$$

$$d_1 = (S^{\mathrm{m}}_{16} - S^{\mathrm{f}}_{16})(a_{11} - a_{66}), \tag{18c}$$

$$d_2 = (S^{\mathrm{m}}_{26} - S^{\mathrm{f}}_{26})(V_{\mathrm{f}} + V_{\mathrm{m}}a_{11})(a_{22} - a_{66}) + (S^{\mathrm{m}}_{16} - S^{\mathrm{f}}_{16})(V_{\mathrm{f}} + V_{\mathrm{m}}a_{66})a_{12}, \tag{18d}$$

$$\beta_{11} = S^{\mathrm{m}}_{12} - S^{\mathrm{f}}_{12}, \qquad \beta_{12} = S^{\mathrm{m}}_{11} - S^{\mathrm{f}}_{11}, \qquad \beta_{22} = (V_{\mathrm{f}} + V_{\mathrm{m}}a_{22})(S^{\mathrm{m}}_{12} - S^{\mathrm{f}}_{12}), \tag{18e}$$

$$\beta_{21} = V_{\mathrm{m}}(S^{\mathrm{f}}_{12} - S^{\mathrm{m}}_{12})a_{12} - (V_{\mathrm{f}} + V_{\mathrm{m}}a_{11})(S^{\mathrm{f}}_{22} - S^{\mathrm{m}}_{22}). \tag{18f}$$

The incremental stresses generated in the fiber and matrix phases are derived as

$$\begin{Bmatrix} \mathrm{d}\sigma^{\mathrm{f}}_{11} \\ \mathrm{d}\sigma^{\mathrm{f}}_{22} \\ \mathrm{d}\sigma^{\mathrm{f}}_{12} \end{Bmatrix} = \begin{bmatrix} b_{11} & b_{12} & b_{16} \\ 0 & b_{22} & b_{26} \\ 0 & 0 & b_{66} \end{bmatrix} \begin{Bmatrix} \mathrm{d}\sigma_{11} \\ \mathrm{d}\sigma_{22} \\ \mathrm{d}\sigma_{12} \end{Bmatrix} = [B] \begin{Bmatrix} \mathrm{d}\sigma_{11} \\ \mathrm{d}\sigma_{22} \\ \mathrm{d}\sigma_{12} \end{Bmatrix}, \tag{19a}$$

and

$$\begin{Bmatrix} \mathrm{d}\sigma^{\mathrm{m}}_{11} \\ \mathrm{d}\sigma^{\mathrm{m}}_{22} \\ \mathrm{d}\sigma^{\mathrm{m}}_{12} \end{Bmatrix} = \begin{bmatrix} a_{11} & a_{12} & a_{16} \\ 0 & a_{22} & a_{26} \\ 0 & 0 & a_{66} \end{bmatrix} \begin{bmatrix} b_{11} & b_{12} & b_{16} \\ 0 & b_{22} & b_{26} \\ 0 & 0 & b_{66} \end{bmatrix} \begin{Bmatrix} \mathrm{d}\sigma_{11} \\ \mathrm{d}\sigma_{22} \\ \mathrm{d}\sigma_{12} \end{Bmatrix} = [A][B] \begin{Bmatrix} \mathrm{d}\sigma_{11} \\ \mathrm{d}\sigma_{22} \\ \mathrm{d}\sigma_{12} \end{Bmatrix}, \tag{19b}$$

where

$$b_{11} = (V_{\mathrm{f}} + V_{\mathrm{m}}a_{22})(V_{\mathrm{f}} + V_{\mathrm{m}}a_{66})/c, \qquad b_{12} = -(V_{\mathrm{m}}a_{12})(V_{\mathrm{f}} + V_{\mathrm{m}}a_{66})/c, \tag{19c}$$

$$b_{16} = [(V_{\mathrm{m}}a_{12})(V_{\mathrm{m}}a_{26}) - (V_{\mathrm{f}} + V_{\mathrm{m}}a_{22})(V_{\mathrm{m}}a_{16})]/c, \qquad b_{22} = (V_{\mathrm{f}} + V_{\mathrm{m}}a_{11})(V_{\mathrm{f}} + V_{\mathrm{m}}a_{66})/c, \tag{19d}$$

$$b_{26} = -(V_{\mathrm{m}}a_{26})(V_{\mathrm{f}} + V_{\mathrm{m}}a_{11})/c, \qquad b_{66} = (V_{\mathrm{f}} + V_{\mathrm{m}}a_{22})(V_{\mathrm{f}} + V_{\mathrm{m}}a_{11})/c, \tag{19e}$$

$$c = (V_{\mathrm{f}} + V_{\mathrm{m}}a_{11})(V_{\mathrm{f}} + V_{\mathrm{m}}a_{22})(V_{\mathrm{f}} + V_{\mathrm{m}}a_{66}). \tag{19f}$$

Note that Eqs. (18a)–(18f) and (19a)–(19f) are valid regardless of any plastic flow theory applied to the fibers and matrix. However, if both the constituents are in elastic deformation, we have $S^{\mathrm{f}}_{16} = S^{\mathrm{f}}_{26} = S^{\mathrm{m}}_{16} = S^{\mathrm{m}}_{26} = 0$, and hence, $b_{16} = b_{26} = a_{16} = a_{26} = 0$.

2.5. Failure criterion [18,20]

As both the internal stresses in the constituents and the overall stresses on the composite are already known, any failure criterion, either applied to isotropic and/or homogeneous materials, or applied to anisotropic and/or heterogeneous materials, can be incorporated to determine the allowable load sustained by the composite. Let us choose a failure criterion that is only employed at the constituent level. Namely, the composite ultimate strength is assumed when any constituent material fails.

The maximum normal stress criterion is among the best of such criteria. It is efficient when the three principal stresses of the material differ from each other significantly. If, however, two or three of them become equal, which can easily occur in the matrix material of a composite, the accuracy of this criterion is certainly questionable. Otherwise, a material would be able to sustain a same amount of equibiaxial or equitriaxial tension as it does uniaxial tension, which might be impossible phenomenologically. In light of this, a generalized criterion to detect tensile failure of the material is expressed as [20]

$$\sigma_{\mathrm{eq}} \geq \sigma_{\mathrm{u}}, \tag{20a}$$

where

$$\sigma_{\mathrm{eq}} = \begin{cases} \sigma^1, & \text{when } \sigma^3 < 0 \\ [(\sigma^1)^q + (\sigma^2)^q]^{1/q}, & \text{when } \sigma^3 = 0 \\ [(\sigma^1)^q + (\sigma^2)^q + (\sigma^3)^q]^{1/q} & \text{when } \sigma^3 > 0, \\ 1 < q \leq \infty \end{cases} \tag{20b}$$

In the above, σ^1, σ^2, and σ^3 are the three principal stresses of the material with $\sigma^1 \geq \sigma^2 \geq \sigma^3$ and σ_{u} is the ultimate tensile strength of the material under a uniaxial load. It is seen that when the power-index $q = \infty$, (20a) together with (20b) is equivalent to the maximum normal stress criterion. In a subsequent example, a comparison study will show that $q = 3$ is pertinent. Thus, the difference between the generalized and the classical maximum normal stress criteria is distinct only when the second or the third principal stress of the material is close to its first principal stress.

In contrast to multiaxial tensions, an equitriaxial compression on an isotropic material can hardly cause it to fail. Hence, a criterion to govern the compressive failure of the material is simply given by

$$\sigma^3 \leq (-\sigma_{\mathrm{u,c}}), \tag{21}$$

where $\sigma_{\mathrm{u,c}}$ is the ultimate compressive strength of the material under a uniaxial load. It should be pointed out that no material buckling is assumed in the compression concerned herein. Further, the material parameters used in Eqs. (7a)–(7c) may be different, under compression, from those under tension.

2.6. Strength formulae under uniaxial loads [24]

Suppose that the fibers used are linearly elastic until rupture and the matrix is bilinearly elastic–plastic. From Eqs. (19a) and (19b) with $\beta = \alpha = 0.5$, and based on the classical maximum normal stress criterion, closed form strength formulae for UD composites under different uniaxial loads are derived as follows [24].

The ultimate strength only due to a longitudinal tensile load (σ_{11}) is given by

$$\sigma_{11}^{\mathrm{u}} = \min\left\{ \frac{\sigma_{\mathrm{u}}^{\mathrm{f}} - (\alpha_{\mathrm{e1}}^{\mathrm{f}} - \alpha_{\mathrm{p1}}^{\mathrm{f}})\sigma_{11}^{0}}{\alpha_{\mathrm{p1}}^{\mathrm{f}}}, \frac{\sigma_{\mathrm{u}}^{\mathrm{m}} - (\alpha_{\mathrm{e1}}^{\mathrm{m}} - \alpha_{\mathrm{p1}}^{\mathrm{m}})\sigma_{11}^{0}}{\alpha_{\mathrm{p1}}^{\mathrm{m}}} \right\}, \tag{22a}$$

where

$$\sigma_{11}^{0} = \min\left\{ \frac{\sigma_{\mathrm{Y}}^{\mathrm{m}}}{\alpha_{\mathrm{e1}}^{\mathrm{m}}}, \frac{\sigma_{\mathrm{u}}^{\mathrm{f}}}{\alpha_{\mathrm{e1}}^{\mathrm{f}}} \right\}, \tag{22b}$$

$$\alpha_{\mathrm{e1}}^{\mathrm{f}} = \frac{E_{11}^{\mathrm{f}}}{V_{\mathrm{f}}E_{11}^{\mathrm{f}} + (1 - V_{\mathrm{f}})E^{\mathrm{m}}}, \tag{22c}$$

$$\alpha_{\mathrm{e1}}^{\mathrm{m}} = \frac{E^{\mathrm{m}}}{V_{\mathrm{f}}E_{11}^{\mathrm{f}} + (1 - V_{\mathrm{f}})E^{\mathrm{m}}}, \tag{22d}$$

$$\alpha_{\mathrm{p1}}^{\mathrm{f}} = \frac{E_{11}^{\mathrm{f}}}{V_{\mathrm{f}}E_{11}^{\mathrm{f}} + (1 - V_{\mathrm{f}})E_{\mathrm{T}}^{\mathrm{m}}}, \tag{22e}$$

$$\alpha_{\mathrm{p1}}^{\mathrm{m}} = \frac{E_{\mathrm{T}}^{\mathrm{m}}}{V_{\mathrm{f}}E_{11}^{\mathrm{f}} + (1 - V_{\mathrm{f}})E_{\mathrm{T}}^{\mathrm{m}}}. \tag{22f}$$

The ultimate strength only due to a transverse tensile load (σ_{22}) is determined from

$$\sigma_{22}^{\mathrm{u}} = \min\left\{ \frac{\sigma_{\mathrm{u}}^{\mathrm{f}} - (\alpha_{\mathrm{e2}}^{\mathrm{f}} - \alpha_{\mathrm{p2}}^{\mathrm{f}})\sigma_{22}^{0}}{\alpha_{\mathrm{p2}}^{\mathrm{f}}}, \frac{\sigma_{\mathrm{u}}^{\mathrm{m}} - (\alpha_{\mathrm{e2}}^{\mathrm{m}} - \alpha_{\mathrm{p2}}^{\mathrm{m}})\sigma_{22}^{0}}{\alpha_{\mathrm{p2}}^{\mathrm{m}}} \right\}, \tag{23a}$$

where

$$\sigma_{22}^{0} = \min\left\{ \frac{\sigma_{\mathrm{Y}}^{\mathrm{m}}}{\alpha_{\mathrm{e2}}^{\mathrm{m}}}, \frac{\sigma_{\mathrm{u}}^{\mathrm{f}}}{\alpha_{\mathrm{e2}}^{\mathrm{f}}} \right\}, \tag{23b}$$

$$\alpha_{\mathrm{e2}}^{\mathrm{f}} = \frac{E_{22}^{\mathrm{f}}}{V_{\mathrm{f}}E_{22}^{\mathrm{f}} + 0.5(1 - V_{\mathrm{f}})(E^{\mathrm{m}} + E_{22}^{\mathrm{f}})}, \tag{23c}$$

$$\alpha_{\mathrm{e2}}^{\mathrm{m}} = \frac{0.5(E_{22}^{\mathrm{f}} + E^{\mathrm{m}})}{V_{\mathrm{f}}E_{22}^{\mathrm{f}} + 0.5(1 - V_{\mathrm{f}})(E^{\mathrm{m}} + E_{22}^{\mathrm{f}})}, \tag{23d}$$

$$\alpha_{\mathrm{p2}}^{\mathrm{f}} = \frac{E_{22}^{\mathrm{f}}}{V_{\mathrm{f}}E_{22}^{\mathrm{f}} + 0.5(1 - V_{\mathrm{f}})(E_{\mathrm{T}}^{\mathrm{m}} + E_{22}^{\mathrm{f}})}, \tag{23e}$$

$$\alpha_{\mathrm{p2}}^{\mathrm{m}} = \frac{0.5(E_{22}^{\mathrm{f}} + E_{\mathrm{T}}^{\mathrm{m}})}{V_{\mathrm{f}}E_{22}^{\mathrm{f}} + 0.5(1 - V_{\mathrm{f}})(E_{\mathrm{T}}^{\mathrm{m}} + E_{22}^{\mathrm{f}})}. \tag{23f}$$

The ultimate strength only due to an in-plane shear load (σ_{12}) reads

$$\sigma_{12}^{u} = \min\left\{ \frac{\sigma_u^f - (\alpha_{e3}^f - \alpha_{p3}^f)\sigma_{12}^0}{\alpha_{p3}^f}, \frac{\sigma_u^m - (\alpha_{e3}^m - \alpha_{p3}^m)\sigma_{12}^0}{\alpha_{p3}^m} \right\}, \tag{24a}$$

where

$$\sigma_{12}^0 = \min\left\{ \frac{\sigma_Y^m}{\sqrt{3}\alpha_{e3}^m}, \frac{\sigma_u^f}{\alpha_{e3}^f} \right\}, \tag{24b}$$

$$\alpha_{e3}^f = \frac{G_{12}^f}{V_f G_{12}^f + 0.5(1 - V_f)(G^m + G_{12}^f)}, \tag{24c}$$

$$\alpha_{e3}^m = \frac{0.5(G_{12}^f + G^m)}{V_f G_{12}^f + 0.5(1 - V_f)(G^m + G_{12}^f)}, \tag{24d}$$

$$\alpha_{p3}^f = \frac{3G_{12}^f}{3V_f G_{12}^f + 0.5(1 - V_f)(E_T^m + 3G_{12}^f)}, \tag{24e}$$

$$\alpha_{p3}^m = \frac{0.5(3G_{12}^f + E_T^m)}{3V_f G_{12}^f + 0.5(1 - V_f)(E_T^m + 3G_{12}^f)}. \tag{24f}$$

It is noted that the above equations have not incorporated any effect of thermal residual stresses. The strength formulae with thermal residual stress influence have been given in Ref. [25].

2.7. Thermal analysis [25,28]

Let T_1 represent the working temperature of the composite, and T_0 the reference temperature at which the internal stresses of the fiber and the matrix are both known (e.g. zero). Due to mismatch between the thermal expansion coefficients of the fibers and the matrix, thermal stresses will be generated in the constituent materials during the temperature variation, $dT = T_1 - T_0$. The general constitutive equations of the fiber, matrix, and the composite are modified to

$$\{d\varepsilon_i^f\} = [S_{ij}^f]\{d\sigma_j^f\} + \{\alpha_i^f\}dT, \tag{25a}$$

$$\{d\varepsilon_i^m\} = [S_{ij}^m]\{d\sigma_j^m\} + \{\alpha_i^m\}dT, \tag{25b}$$

and

$$\{d\varepsilon_i\} = [S_{ij}]\{d\sigma_j\} + \{\alpha_i\}dT. \tag{25c}$$

where α_i^f, α_i^m, and α_i, respectively, denote the thermal expansion coefficients of the fiber, matrix, and the composite at the initial temperature T_0 with $\alpha_3^f = \alpha_2^f$, $\alpha_3^m = \alpha_2^m = \alpha_1^m$, and $\alpha_4^f = \alpha_5^f = \alpha_6^f = \alpha_4^m = \alpha_5^m = \alpha_6^m = 0$. It should be noted that the compliance matrices in (25a) and (25b), $[S_{ij}^f]$ and $[S_{ij}^m]$, are also defined at the initial temperature T_0, which may not be merely the elastic components.

On the other hand, we have (see Eqs. (4a) and (4b))

$$\{d\sigma_i^f\} = (V_f[I] + V_m[A_{ij}])^{-1}\{d\sigma_j\} + \{b_i^f\}dT = [B_{ij}^f]\{d\sigma_j\} + \{b_i^f\}dT, \tag{26a}$$

$$\{d\sigma_1^m\} = [A_{ij}](V_f[I] + V_m[A_{ij}])^{-1}\{d\sigma_j\} + \{b_i^m\}dT = [B_{ij}^m]\{d\sigma_j\} + \{b_i^m\}dT. \tag{26b}$$

$\{b_i^f\}$ and $\{b_i^m\}$ are called thermal stress concentration factors of the fiber and the matrix, satisfying

$$V_f\{b_i^f\} + V_m\{b_i^m\} = \{0\}. \tag{27}$$

Both Levin (see Refs. [25,45]) and Benveniste and Dvorak (Refs. [28,46]) have found rigorous expressions for the composite thermal expansion coefficients by making use of the constituent concentration matrices, $[B_{ij}^f]$ and $[B_{ij}^m]$. Choosing $\{b_i^m\}$ as independent, the Benveniste and Dvorak formula reads [46]

$$\{b_i^m\} = ([I] - [B_{ij}^m])([S_{ij}^f] - [S_{ij}^m])^{-1}(\{\alpha_j^m\} - \{\alpha_j^f\}).$$

By means of the bridging matrix, the last equation becomes

$$\{b_i^m\} = ([I] - [A_{ij}](V_f[I] + V_m[A_{ij}])^{-1})([S_{ij}^f] - [S_{ij}^m])^{-1} \times (\{\alpha_j^m\} - \{\alpha_j^f\}). \tag{28}$$

The overall thermal expansion coefficients of the composite are determined from

$$\{\alpha_i\} = V_f\{\alpha_i^f\} + V_m\{\alpha_i^m\} + V_m([S_{ij}^m] - [S_{ij}^f])\{b_j^m\}. \tag{29}$$

If there is no overall load applied to the lamina, namely, $\{d\sigma_j\} = \{0\}$, the pure thermal stress increments in the constituents are simply given by

$$\{d\sigma_i^m\}^{(T)} = \{b_i^m\}dT \quad \text{and} \quad \{d\sigma_i^f\}^{(T)} = -\frac{V_m}{V_f}\{b_i^m\}dT. \tag{30}$$

Total stresses increments in the constituents are obtained by firstly performing an isothermal analysis and then a pure thermal analysis.

3. Simulation of unidirectional laminae

3.1. Effective elastic moduli [16,21,23]

It can be recognized from the above model development that the unique feature of the present model is in the explicit determination of averaged internal stresses in the constituent fiber and matrix materials until rupture. For this purpose, a bridging matrix has been employed. The most important task is to determine the independent bridging elements in Eq. (6). As elaborated in Appendix B, the independent bridging elements can only depend on the material properties of the constituents and on the fiber packing geometry in the

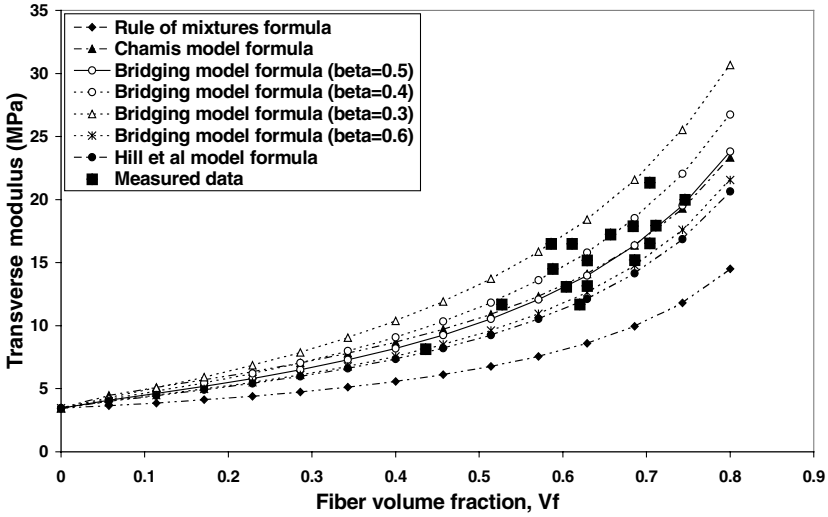

Fig. 1. Predicted and measured [47] transverse moduli of UD composites versus fiber volume fraction. The material parameters used are: $E^{\mathrm{f}} = 73.1$ GPa, $\nu^{\mathrm{f}} = 0.22$, $E^{\mathrm{m}} = 3.45$ GPa, and $\nu^{\mathrm{m}} = 0.35$.

matrix. As long as the composite elastic responses obtained based on these independent elements are correct, the validity of these elements with varied material properties when applied to a composite inelastic response analysis can be expected (Appendix B). It is thus of critical importance to check the accuracy of the resulting formulae, Eqs. (11a)–(11e), for the composite engineering moduli.

The longitudinal Young's modulus and Poisson's ratio formulae, Eqs. (11a) and (11b), are the same as rule of mixtures formulae, which are sufficiently accurate for most unidirectional composites. Hence, the corresponding bridging elements, Eqs. (7a) and (7d), are generally valid. On the other hand, the composite transverse and in-plane shear responses are much more sensitive to the specific fiber packing geometry. Accordingly, the parameters β and α, which are called as Bridging Parameters for convenience, stand for the influences of this packing geometry. It is important to realize that these bridging parameters are independent of material properties.

A UD composite made using isotropic glass fibers and epoxy matrix with $E^{\mathrm{f}} = 73.1$ GPa, $E^{\mathrm{m}} = 3.45$ GPa, $\nu^{\mathrm{f}} = 0.22$, and $\nu^{\mathrm{m}} = 0.35$ is used for both analytical prediction and experiment to obtain the transverse modulus E_{22} of the composite. The results are shown in Fig. 1 in which the experimental data are taken from Ref. [47]. For comparison, predictions by using other two established micromechanics model formulae, the Chamis model [48] and the Hill–Hashin–Christensen–Lo model [49] formulae, are also

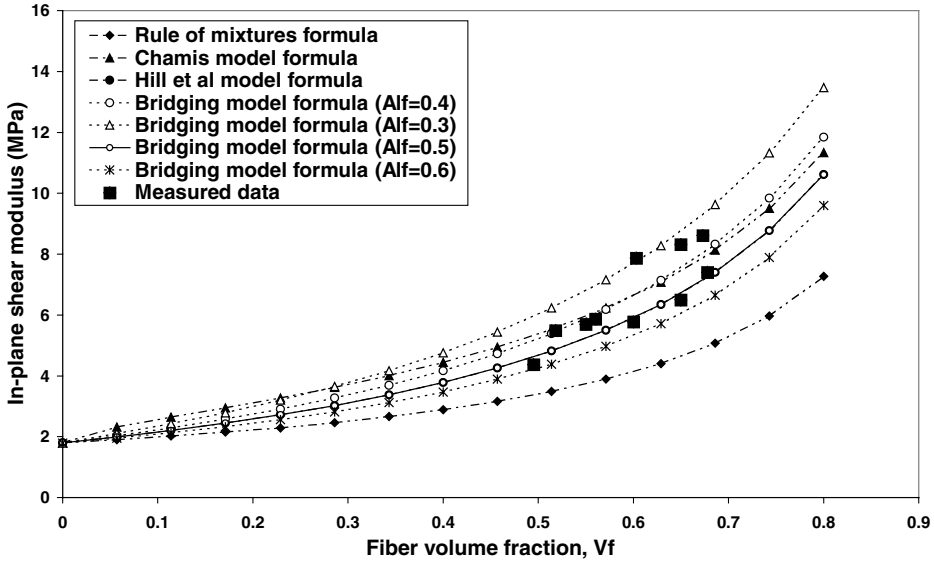

Fig. 2. Predicted and measured [47] in-plane shear moduli of UD composites versus fiber volume fraction. The material parameters used are: $G^{\mathrm{f}} = 30.2$ GPa and $G^{\mathrm{m}} = 1.8$ GPa.

Table 1
Thermal–mechanical properties of four UD laminae [50] ($\beta = 0.45$ and $\alpha = 0.35$)

		Composite 1	Composite 2	Composite 3	Composite 4
Fiber volume fraction, V_f		0.60	0.60	0.62	0.60
Fiber properties [50]	Type	AS4	T300	E-glass 21 × K43 Gevetex	Silenka E-Glass 1200tex
	E_{11}^f (GPa)	225	230	80	74
	E_{22}^f (GPa)	15	15	80	74
	G_{12}^f (GPa)	15	15	33.33	30.8
	ν_{12}^f	0.2	0.2	0.2	0.2
	α_1^f ($\times 10^{-6}$/°C)	−0.5	−0.7	4.9	4.9
	α_2^f ($\times 10^{-6}$/°C)	15	12	4.9	4.9
Matrix properties [50]	Type	3501-6 epoxy	BSL914C epoxy	LY556/HT907/DY063 epoxy	MY750/HY917/DY063 epoxy
	E^m (GPa)	4.2	4.0	3.35	3.35
	ν^m	0.34	0.35	0.35	0.35
	α^m ($\times 10^{-6}$/°C)	45	55	58	58
Lamina properties (measured [50])	E_{11} (GPa)	126	138	53.48	45.6
	E_{22} (GPa)	11	11	17.7	16.2
	G_{12} (GPa)	6.6	5.5	5.83	5.83
	ν_{12}	0.28	0.28	0.278	0.278
	α_1 ($\times 10^{-6}$/°C)	−1	−1	8.6	8.6
	α_2 ($\times 10^{-6}$/°C)	26	26	26.4	26.4
Lamina properties (Bridging model prediction)	E_{11} (GPa)	136.7	139.6	50.87	45.74
	E_{22} (GPa)	9.23	9.09	14.38	13.45
	G_{12} (GPa)	5.54	5.04	5.72	5.31
	ν_{12}	0.256	0.26	0.257	0.26
	α_1 ($\times 10^{-6}$/°C)	0.06	−0.06	6.23	6.46
	α_2 ($\times 10^{-6}$/°C)	27.9	29.6	20.62	21.67
Schapery's prediction	α_1 ($\times 0^{-6}$/°C)	0.06	−0.06	6.23	6.46
	α_2 ($\times 10^{-6}$/°C)	33.04	36.83	31.8	33.17

shown in the figure. It is seen that for this composite, the bridging model predictions based on $0.4 \leq \beta < 0.5$ are in closest agreement with the experiments. It is also seen that the smaller the parameter β used the stiffer the predicted modulus will be. To obtain comparison for the shear modulus G_{12}, another glass/epoxy composite with $G^f = 30.2$ GPa and $G^m = 1.8$ GPa is used. The experimental data for G_{12}, also taken from Ref. [47], are plotted in Fig. 2 to compare with the predicted results based on the bridging model, the Chamis model, and the Hill–Hashin model. Similar evidences have been observed. It is noted that the bridging model formula with $\alpha = 0.5$ is identical with the Hill–Hashin formula for the in-plane shear modulus. Other comparisons are listed in Table 1, and more in Refs. [16,21,23].

3.2. Overall thermal expansion coefficients [28,29]

Overall thermal expansion coefficients of four polymer-matrix based UD composites were calculated, using independently measured constituent properties of the composites reported in Ref. [50], and are listed in Table 1. For comparison, predictions by using Schapery's formulae [51] were also made, and are reported in the table. It is seen that the overall longitudinal thermal expansion coefficients from these two models are identical, whereas the present predictions for the transverse coefficients are more accurate than Schapery's model predictions. It should be noted that Schapery's formula can be derived based on an assumption of free transverse thermal-stress components in the constituent materials [47], whereas the present formulae, Eq. (26) or Eq. (30), also give nonzero transverse thermal stresses in the constituents. The latter is seen to be consistent with a three-dimensional FEM solution [52].

In all the following calculations, the bridging parameters are chosen as $\beta = \alpha = 0.5$.

3.3. Elasto-plastic response [17,22]

Two boron (B) fiber reinforced aluminum (Al) UD composites were studied for this purpose. For the first composite, Brockenbrough et al. [15] employed a FEM (finite element method) technique to investigate the influence of fiber arrangement and fiber cross-sectional shape on its elastic–plastic response. The boron fiber was considered as isotropically linear elastic until rupture while the aluminum matrix as elastic–plastic. They found that little influence exists in the elastic region. The same is true for the

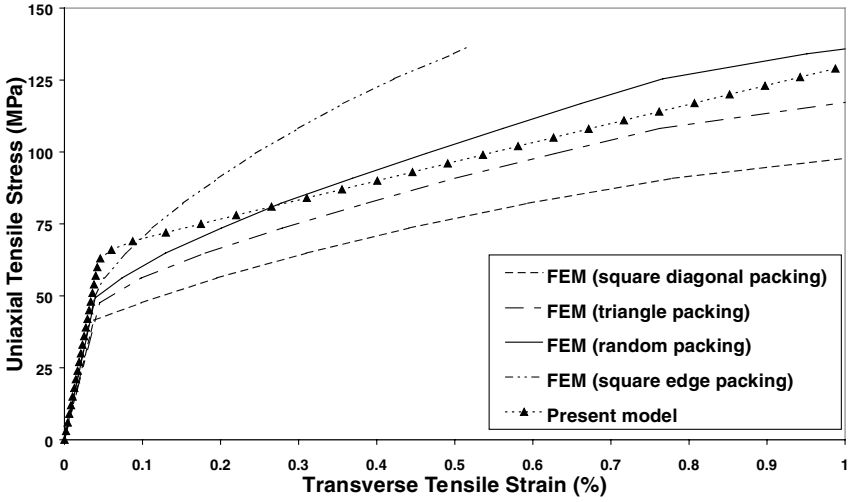

Fig. 3. Comparison of different solutions to the transverse elastic–plastic response of a boron/aluminium composite ($V_f = 0.46$). The FEM solutions were taken from Ref. [15].

longitudinal plastic response when a tensile load is applied longitudinally. However, the conclusion is no longer valid for the transverse plastic response. The most significant influence is on the transverse tensile and in-plane shear deformation due to different fiber arrangements. In their modeling, four fiber arrangement patterns, i.e. square diagonal packing, triangle packing, random packing, and square edge packing, were considered. With random packing assumption, the FEM solution gave results closest to the experimental data [53]. This is unsurprising, since any regular arrangement assumption for the fibers is generally not found in a real composite. The predicted results of the present model were comparable with the random packing FEM solution, as indicated in Fig. 3. In the present calculation, the following parameters were directly taken from Ref. [15]: $E^f = 410$ GPa, $\nu^f = 0.2$, $E^m = 69$ GPa, $\nu^m = 0.33$, $\sigma_Y^m = 43$ MPa, and $V_f = 0.46$. The matrix hardening modulus, however, was measured from the testing curve reported in Ref. [15, Fig. 2]. Three linear segments were used to represent the plastic hardening curve of the aluminum matrix. The used matrix hardening modulus is given as:

$$E_T^m = \begin{cases} 1.88 \text{ GPa}, & \text{when } 43 \text{ MPa} < \sigma_e^m \le 93.6 \text{ MPa} \\ 0.66 \text{ GPa}, & \text{when } 93.6 \text{ MPa} < \sigma_e^m \le 123.8 \text{ MPa} \\ 0.17 \text{ GPa}, & \text{when } \sigma_e^m > 123.8 \text{ MPa} \end{cases}$$

The second B-Al UD composite is subjected to combined axial tension and torsion loads. Experimental data for this composite are taken from a part of the results reported in Ref. [54]. The whole load sequence consisted of several load paths, some of which were reversed in load directions from the others, see Ref. [54, Figs. 11 and 12] for details. In order to simulate this complicated load sequence, a number of load intervals have been chosen in which some intervals are considered as loading while the others as unloading. Whenever there is one stress component (called key stress component), which begins to change its direction, it is considered to begin a new loading or unloading interval. Each loading or unloading process continues till the key stress component reaches zero. Then a reversed unloading

Table 2
Key points in the load sequence of a boron/aluminium UD composite used for elastic–plastic response analysis

Load sequence: O to A (loading); A to B (loading); B to B′ (unloading); B′ to C (loading); C to D (unloading); D to D′ (unloading); D′ to E (loading); E to E′ (unloading); E′ to F (loading); F to F′ (unloading); F′ to G (loading); G to H (unloading); H to J (loading); J to K (loading); K to K′ (unloading); K′ to L (loading)

Point	Magnitude		Point	Magnitude		Point	Magnitude	
	σ_{11} (MPa)	σ_{21} (MPa)		σ_{11} (MPa)	σ_{21} (MPa)		σ_{11} (MPa)	σ_{21} (MPa)
O	0	0	A	0	18	B	0	54
B′	0	0	C	0	−62	D	62	−52
D′	62	0	E	62	64	E′	62	0
F	62	−63.4	F′	62	0	G	62	4
H	48	0	J	180	0	K	180	73
K′	180	0	L	180	−69			

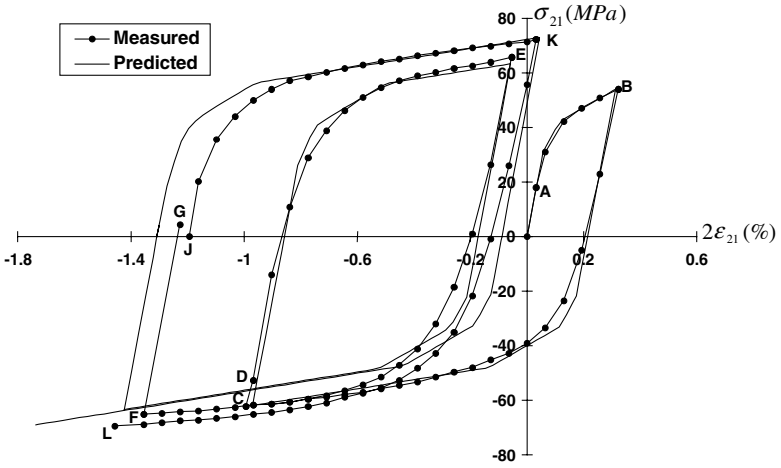

Fig. 4. Predicted and measured [54] shear stress–shear strain response of a boron/aluminium composite under combined tension–torsion loads.

or loading process is considered to start. Details for loading and unloading intervals are listed in Table 2 in which endpoint values of the intervals are also included. These values were measured from Ref. [54, Figs. 11, 12 and 26].

It is known that the in-situ matrix properties depend on the composite processing condition, and may be different from the bulk matrix properties [55]. Also, the yield strengths of a material in different load directions are usually different. Because of no relevant data available from Ref. [54], three piece-wise linear segments were used to approximate the tensile stress–strain curve of the aluminum plotted in Ref. [54, Fig. 27] to obtain the matrix hardening moduli. The elastic constants of boron were inversely calculated from the overall lamina properties given in Ref. [54, Table 1], by using Eq. (11). The experimental stress–strain curves of the first two load paths, shown in Ref. [54, Fig. 26] were used to adjust the matrix yield strengths corresponding to the positive and the negative shear loads. The material properties thus obtained are: $E^{\mathrm{f}} = E_{\mathrm{T}}^{\mathrm{f}} = 445$ GPa, $\nu^{\mathrm{f}} = 0.17$, $E^{\mathrm{m}} = 72.39$ GPa, $\nu^{\mathrm{m}} = 0.33$, and

$$E_{\mathrm{T}}^{\mathrm{m}} = \begin{cases} 23.1\ \mathrm{GPa}, & \text{when } \sigma_{\mathrm{Y}}^{\mathrm{m}} < \sigma_{\mathrm{e}}^{\mathrm{m}} \le \sigma_{\mathrm{Y}}^{\mathrm{m}} + 14\ \mathrm{MPa} \\ 6.9\ \mathrm{GPa}, & \text{when } \sigma_{\mathrm{Y}}^{\mathrm{m}} + 14\ \mathrm{MPa} < \sigma_{\mathrm{e}}^{\mathrm{m}} \le \sigma_{\mathrm{Y}}^{\mathrm{m}} + 32\ \mathrm{MPa} \\ 1.9\ \mathrm{GPa}, & \text{when } \sigma_{\mathrm{e}}^{\mathrm{m}} > \sigma_{\mathrm{Y}}^{\mathrm{m}} + 32\ \mathrm{MPa} \end{cases}$$

where $\sigma_{\mathrm{Y}}^{\mathrm{m}} = 40$ MPa for the positive shear and $\sigma_{\mathrm{Y}}^{\mathrm{m}} = 30$ MPa for the negative shear loads. This difference in yield strengths under shear loads may be attributed to the thermal residual stresses in the composite. The present prediction, however, did not consider any thermal residual stress effect due to no processing information (including stress-free temperature and constituent thermal–mechanical properties at different temperatures) available. The fiber volume fraction, V_{f}, is 0.45 [54]. The predicted results using these parameters together with the experimental data, which were taken from Ref. [54], are plotted in Fig. 4. It can be seen from the figure that most parts of the stress–strain curves from the prediction and the experiment agree quite well.

3.4. Off-axial strength [17,21–23,34]

Ultimate strength is a critical parameter for composite design. Prediction of this strength can be simply achieved using the bridging model. Let us consider a UD composite of glass/epoxy system subjected to an off-axial load. Its constituent elastic properties together with fiber volume fraction, taken from Ref. [56], are summarized in Table 3. No additional constituent properties were reported. These properties can be retrieved from the overall composite strengths in two different directions, e.g. longitudinal strength (X) and transverse strength (Y).

The recovering is begun by assuming that the glass fiber is linearly elastic until rupture, and that the matrix plasticity, if any, consists of bilinear segments. As the stiffness and strength of the glass fiber are much higher than those of the epoxy matrix, Eqs. (23a)–(23f) indicate that the transverse tensile strength of the composite is governed by the strength

Table 3
Parameters of a glass/epoxy UD composite used for off-axial strength analysis ($X = 1236$ MPa, $Y = 28.45$ MPa, $S = 38$ MPa) (X = longitudinal tensile strength, Y = transverse tensile strength, S = in-plane shear strength)

Material	Volume fraction	E_{11} (GPa)	E_{22} (GPa)	ν_{12}	ν_{23}	G_{12} (GPa)	E_{T} (GPa)	σ_{Y} (MPa)	σ_{u} (MPa)
Glass	0.6	73	73	0.22	0.22	29.92	73	2047	2047
Epoxy	0.4	3.45	3.45	0.35	0.35	1.28	–	–	19

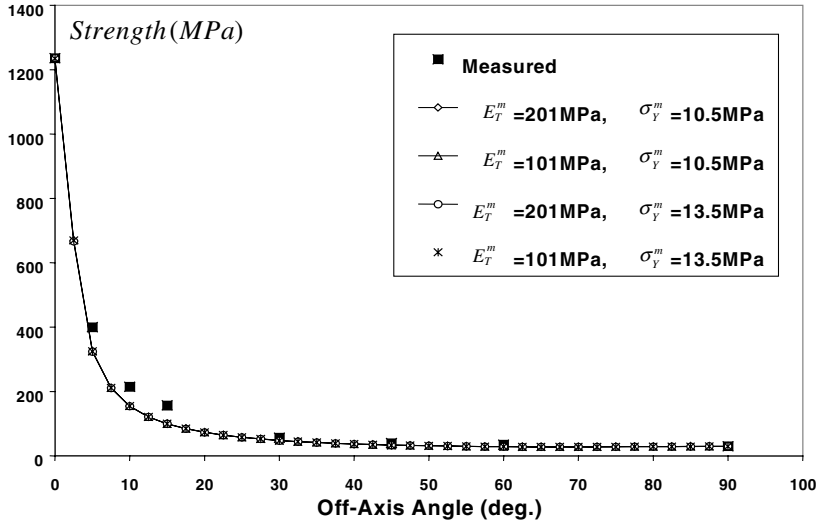

Fig. 5. Predicted and measured [56] off-axial strength of a unidirectional glass/epoxy composite. The parameters used are: $E^{\mathrm{f}} = E_{\mathrm{T}}^{\mathrm{f}} = 73$ GPa, $E^{\mathrm{m}} = 3.45$ GPa, $\nu_{\mathrm{f}} = 0.22$, $\nu_{\mathrm{m}} = 0.35$, $\sigma_{\mathrm{u}}^{\mathrm{f}} = \sigma_{\mathrm{Y}}^{\mathrm{f}} = 2047$ MPa, $V_{\mathrm{f}} = 0.6$, and $\sigma_{\mathrm{u}}^{\mathrm{m}} = 19$ MPa.

of the matrix. Thus, Eq. (23a) gives

$$\sigma_{22}^{\mathrm{u}} = \frac{\sigma_{\mathrm{Y}}^{\mathrm{m}}}{\alpha_{\mathrm{e2}}^{\mathrm{m}}} + \frac{\sigma_{\mathrm{u}}^{\mathrm{m}} - \sigma_{\mathrm{Y}}^{\mathrm{m}}}{\alpha_{\mathrm{p2}}^{\mathrm{m}}} = Y \approx \frac{\sigma_{\mathrm{u}}^{\mathrm{m}}}{\alpha_{\mathrm{e2}}^{\mathrm{m}}}, \tag{31}$$

since $\alpha_{\mathrm{p2}}^{\mathrm{m}} \approx \alpha_{\mathrm{e2}}^{\mathrm{m}}$. From Eq. (31), the matrix strength is recovered to be 18.4 MPa (a slight amendment is later made for the recovered parameter due to incorporation of matrix plasticity, i.e. $\alpha_{\mathrm{p2}}^{\mathrm{m}} \neq \alpha_{\mathrm{e2}}^{\mathrm{m}}$, see Table 3). Next, let us use Eq. (22a) to recover the fiber strength. It is required that

$$\sigma_{11}^{\mathrm{u}} = \min\left\{ \frac{\sigma_{\mathrm{u}}^{\mathrm{f}} - (\alpha_{\mathrm{e1}}^{\mathrm{f}} - \alpha_{\mathrm{p1}}^{\mathrm{f}})\sigma_{11}^{0}}{\alpha_{\mathrm{p1}}^{\mathrm{f}}}, \frac{\sigma_{\mathrm{u}}^{\mathrm{m}} - (\alpha_{\mathrm{e1}}^{\mathrm{m}} - \alpha_{\mathrm{p1}}^{\mathrm{m}})\sigma_{11}^{0}}{\alpha_{\mathrm{p1}}^{\mathrm{m}}} \right\} = X.$$

At this stage, we cannot assume that $\alpha_{\mathrm{p1}}^{\mathrm{m}} \approx \alpha_{\mathrm{e1}}^{\mathrm{m}}$. However, the longitudinal strength of the composite is most probably governed by the strength of the fiber especially when the fiber volume fraction is high. Thus, we can consider $X = \sigma_{11}^{\mathrm{u}} \approx \sigma_{\mathrm{u}}^{\mathrm{f}}/\alpha_{\mathrm{e1}}^{\mathrm{f}}$, due to $\alpha_{\mathrm{p1}}^{\mathrm{f}} \approx \alpha_{\mathrm{e1}}^{\mathrm{f}}$, provided that we can choose the other two parameters of the matrix, $E_{\mathrm{T}}^{\mathrm{m}}$ and $\sigma_{\mathrm{Y}}^{\mathrm{m}}$, such that

$$\left(\frac{\sigma_{\mathrm{Y}}^{\mathrm{m}}}{\alpha_{\mathrm{e1}}^{\mathrm{m}}} + \frac{\sigma_{\mathrm{u}}^{\mathrm{m}} - \sigma_{\mathrm{Y}}^{\mathrm{m}}}{\alpha_{\mathrm{p1}}^{\mathrm{m}}} \right)_{\sigma_{\mathrm{u}}^{\mathrm{m}} = 18.4\ \mathrm{MPa}} \geq X. \tag{32}$$

It is clear that many different combinations of $E_{\mathrm{T}}^{\mathrm{m}}$ and $\sigma_{\mathrm{Y}}^{\mathrm{m}}$, which satisfy inequality (32), exist. Since $(\sigma_{\mathrm{u}}^{\mathrm{m}}/\alpha_{\mathrm{e1}}^{\mathrm{m}})_{\sigma_{\mathrm{u}}^{\mathrm{m}}=18.4\ \mathrm{MPa}} < X$, the epoxy used cannot be considered as linearly elastic until rupture. On the other hand, any combination of $E_{\mathrm{T}}^{\mathrm{m}}$ and $\sigma_{\mathrm{Y}}^{\mathrm{m}}$, which satisfy (32), can be regarded as the matrix plastic parameters due to no other information. Calculated results for the off-axial tensile strength of the composite with four different combinations of $E_{\mathrm{T}}^{\mathrm{m}}$ and $\sigma_{\mathrm{Y}}^{\mathrm{m}}$ are plotted in Fig. 5, which are compared with experimental data taken from Ref. [56]. It is seen that all the four curves almost coincide with each other. This may be attributed to the fact that the ultimate strength of the composite is mainly dependent on the ultimate stresses, but less on the yield strength or hardening modulus, of the constituent materials, although the ultimate strain and the entire stress–strain curve of the composite do depend on them. This is especially true when the modular ratio of the two constituent materials is large. It should be pointed out that the conclusion made herein is only applicable to UD composites which are statically determinate. For an angle-plied lamina in the laminate which is statically indeterminate, its strength prediction depends heavily on its plastic properties [26], see also the subsequent section for details. Other examples of off-axial strength predictions have been reported elsewhere [17,21–23,34].

3.5. Tensile strength at elevated temperature [22]

Metal matrix composites usually have high service temperature. When these composites are subjected to a mechanical load, the ultimate strength of the composites varies with both the elevated temperature and the external load. In this example, a ceramic alumina fiber reinforced aluminum matrix composite was investigated, having a fiber volume fraction of $V_{\mathrm{f}} = 0.5$. The measured off-axial tensile strengths of this composite at a number of temperatures from room temperature to 773 K were performed by Matsuda and Matsuura [57]. The alumina fibers (being linearly elastic until rupture) were considered as temperature independent [58], and its thermal–elastic properties were taken from Ref. [58]. On the other hand, the properties of the aluminum matrix depend on temperature heavily, and were taken, except for the tensile strengths, from Ref. [59]. Thus, only the constituent strengths at each temperature were recovered from some overall strengths of the composite. However, the alumina strength is temperature

Table 4
Material properties of the alumina/aluminium UD composite ($V_f = 0.5$) used for elevated temperature off-axial strength analysis: properties of alumina fibers, independent of temperature [58]

Young's modulus (GPa)	Tensile strength (MPa)	Poisson's ratio	Thermal expansion coefficient ($\times 10^{-6}$/K)
300	1380	0.26	6.0

independent. Only the longitudinal tensile strength of the composite at room temperature was used to retrieve the fiber strength. Because the matrix plastic parameters had already been chosen, this retrieval was easy to perform, by simply setting the fiber strength equal to the resulting maximum normal stress in the fiber when applying a longitudinal tensile load to the composite. This longitudinal tensile load should be equal to the composite longitudinal tensile strength. The aluminum matrix tensile strength, however, is very temperature dependent. Its strength at each temperature was backed out using the overall transverse tensile strength of the composite at the corresponding temperature. The constituent properties thus obtained are summarized in Tables 4 and 5. The predicted and measured [57] off-axial tensile strengths at temperature of 773 K are plotted in Fig. 6. Good correlation is seen to exist. Further results are referred to Ref. [22].

3.6. Fatigue strength prediction [30]

It is believed that any failure of a material results from its internal stresses, no matter what kind of load has been applied to the material. As such, the overall fatigue strength of a fibrous composite can be similarly estimated by using the Bridging Model, based on the information of the fatigue behaviors of the constituent fiber and matrix materials. Two UD composites are investigated for this purpose. One is a graphite/epoxy (AS/3501-5A) lamina, with a fiber volume fraction of 0.7, and another is a glass/epoxy lamina, with a fiber volume fraction of 0.6. Awerbuch and Hahn [60] made extensive experiments on the first composite, whereas Hashin and Rotem [56] measured the S–N curves of the second lamina, both under off-axial tensile fatigue loads. As no cyclic tests for the constituents were reported, the overall fatigue data of both the composites at some off-axial directions must be used to retrieve the constituent fatigue data. The retrieval is similar to that in obtaining the constituent static parameters. A procedure about this retrieval as per the first example is described below.

First, the scattered fatigue data were best approximated using some polynomial function (a first-order polynomial in the present case). Using the polynomial function, the composite fatigue strength at each off-axial angle corresponding to a given cycle number was determined, as shown in Table 6 (those at $N = 0$ were not shown). From the measured lamina static properties including the lamina longitudinal and transverse tensile strengths, shown in Table 7, the constituent static properties could be backed out, and are listed in Table 8. The elastic properties of the constituents were kept unchanged at every subsequent cyclic load condition, whereas the matrix plastic parameters were kept as constant as possible. At each cycle number, the overall longitudinal and transverse fatigue strengths of the composite were employed to adjust the fiber and matrix strengths, respectively. This adjusting was done as though the same amount of "static loads" had been applied to the composite. If the fiber and matrix strengths could be determined successfully, the matrix plastic parameters were kept unchanged. Otherwise, the matrix yield strength was adjusted accordingly. For example, at a cycle number of $N = 10^3$, the matrix strength, around 26.4 MPa, was firstly determined by applying an equivalent "static" transverse load of 38.5 MPa (see Table 6) to the composite, without changing matrix plastic parameters, i.e. $\sigma_Y^m = 25$ MPa and $E_T^m = 1.8$ GPa (see Table 7). Then, if we loaded the composite longitudinally, we would find that we could not apply to a load level of 1323.7 MPa, which is the composite longitudinal fatigue strength at $N = 10^3$. Thus, the matrix plastic parameters must be adjusted. Keeping the hardening modulus of $E_T^m = 1.8$ GPa unchanged, the yield strength of the matrix was adjusted to 18 MPa. The constituent fatigue parameters thus defined are summarized in Table 8.

Similarly, the constituent fatigue parameters of the second example, glass/epoxy lamina, were retrieved. The only difference is that the overall S–N data of this latter composite at 60° rather than at 90° (transverse direction) off-axial load were used to determine the matrix fatigue strengths when $N > 0$, since no cyclic tests had been performed for the transverse direction specimens. The

Table 5
Material properties of the alumina/aluminium UD composite ($V_f = 0.5$) used for elevated temperature off-axial strength analysis: properties of aluminium matrix [59]

Temperature (K)	Young's modulus (GPa)	Yield strength (MPa)	Hardening modulus (MPa)	Tensile strength (MPa)	Poisson's ratio	Thermal expansion coefficient ($\times 10^{-6}$/K)
297	68.9	41.4	6500	78.4	0.33	23.4
394	63.8	39.3	4500	65	0.33	23.6
473	59.6	36.5	1150	51	0.33	23.9
573	54.6	32.5	500	34	0.33	24.8
673	48.3	15.9	200	21	0.33	24.8
773	42.0	10.5	80	12.5	0.33	25.7

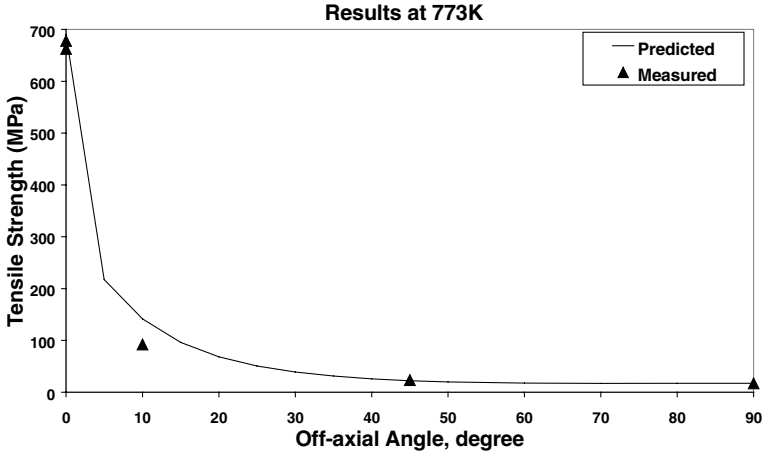

Fig. 6. Predicted and measured [57] off-axial tensile strengths of an alumina fiber and aluminium matrix composite at 773 K. The parameters used are given in Table 4.

retrieved constituent parameters of the glass/epoxy system are given in Table 9.

Using the retrieved constituent fatigue parameters and the respective fiber volume fractions, the predicted off-axial fatigue strengths together with the measured fatigue strengths [60] for the graphite/epoxy composite at $N = 10^3$ and 10^5 are shown in Figs. 7 and 8, whereas the results for the glass/epoxy composite are shown in Fig. 9. More results can be found in Ref. [30]. These figures clearly indicate that the bridging model is efficient for lamina fatigue strength analysis.

4. Simulation of multidirectional laminates

4.1. Classical laminate theory

4.1.1. Iso-thermal analysis [20]

Suppose that the laminated composite consists of multi-layers of UD laminae, each of which has a different ply angle. Let a global coordinate system, (x, y, z), to have its origin on the middle surface of the laminate, with x and y in the laminate plane and z along the thickness direction. Let the fiber direction of the kth lamina have an inclined ply-angle θ_k with the global x direction. In the classical lamination theory, only in-plane stress and strain increments, i.e. $\{\mathrm{d}\sigma\}^{\mathrm{G}} = \{\mathrm{d}\sigma_{xx}, \mathrm{d}\sigma_{yy}, \mathrm{d}\sigma_{xy}\}^{\mathrm{T}}$ and $\{\mathrm{d}\varepsilon\}^{\mathrm{G}} = \{\mathrm{d}\varepsilon_{xx}, \mathrm{d}\varepsilon_{yy}, 2\mathrm{d}\varepsilon_{xy}\}^{\mathrm{T}}$, are retained, where G refers to the global system. The global in-plane strain increments of the laminate at a material point (x, y, z) are expressed as [61]

$$\mathrm{d}\varepsilon_{xx} = \mathrm{d}\varepsilon^0_{xx} + z\mathrm{d}\kappa^0_{xx}, \qquad \mathrm{d}\varepsilon_{yy} = \mathrm{d}\varepsilon^0_{yy} + z\mathrm{d}\kappa^0_{yy},$$

$$2\mathrm{d}\varepsilon_{xy} = 2\mathrm{d}\varepsilon^0_{xy} + 2z\mathrm{d}\kappa^0_{xy},$$

where $\mathrm{d}\varepsilon^0_{xx}$, etc. and $\mathrm{d}\kappa^0_{xx}$, etc. are the strain and the curvature increments of the middle surface, respectively. The global stress increment at the considered material point is obtained from

$$\begin{aligned}\{\mathrm{d}\sigma\}^{\mathrm{G}} &= [C]^{\mathrm{G}}_k\{\mathrm{d}\varepsilon\}^{\mathrm{G}} = [(C^{\mathrm{G}}_{ij})_k]\{\mathrm{d}\varepsilon\}^{\mathrm{G}} \\ &= ([T]_{\mathrm{c}})_k([S]_k)^{-1}([T]^{\mathrm{T}}_{\mathrm{c}})\{\mathrm{d}\varepsilon\}^{\mathrm{G}},\end{aligned} \tag{33}$$

where $[S]_k$ is the compliance matrix of the kth lamina in its local coordinate system given by

$$[S]_k = \begin{bmatrix} S_{11} & S_{12} & S_{16} \\ & S_{22} & S_{26} \\ \text{symmetry} & & S_{66} \end{bmatrix}_k,$$

$$[T_{\mathrm{c}}] = \begin{bmatrix} l_1^2 & l_2^2 & 2l_1l_2 \\ m_1^2 & m_2^2 & 2m_1m_2 \\ l_1m_1 & l_2m_2 & l_1m_2 + l_2m_1 \end{bmatrix}. \tag{34}$$

with $l_1 = m_2 = \cos\theta$, $l_2 = -m_1 = \sin\theta$.

Hence, the averaged stress increments in the kth lamina

Table 6
Material properties of a graphite/epoxy composite ($V_{\mathrm{f}} = 0.7$) under tensile fatigue: measured [60] off-axis fatigue strengths of the composite ($R^* = 0.1$ and $\omega^{**} = 18$ Hz) (* = stress ratio, i.e. $R = \sigma_{\min}/\sigma_{\max}$; ** = cyclic frequency)

Angle	Cyclic number, N			
	10^3	10^4	10^5	10^6
0°	1323.7	1254.6	1185.5	1116.4
10°	295.8	257.6	219.5	181.3
20°	156.6	142.7	128.9	115.1
30°	65.5	68.7	71.9	75.2
45°	67.1	59.5	52.0	44.4
60°	47.0	45.3	43.5	41.8
90°	38.5	36.2	33.9	31.7

Table 7
Material properties of a graphite/epoxy composite ($V_f = 0.7$) under tensile fatigue: static properties (cyclic number, $N = 0$)

	E_{11} (GPa)	E_{22} (GPa)	ν_{12}	G_{12} (GPa)	σ_Y (MPa)	E_T (GPa)	X^a (MPa)	Y^b (MPa)
Fiber	194.3	15.4	0.275	18.1	–	–	2610	–
Matrix	3.45	3.45	0.35	1.28	25	1.8	38.5	–
Lamina (measured [60])	137	9.6	0.3	5.24	–	–	1836	56.9
Lamina (predicted)	137	9.56	0.298	5.24	–	–	1837.6	56.6

[a] Longitudinal tensile strength.
[b] Transverse tensile strength.

can be determined from

$$\{d\sigma\}_k^G = ([T]_c)_k([S]_k)^{-1}([T]_c^T)\{d\varepsilon\}_k^G, \tag{35}$$

where

$$\{d\varepsilon\}_k^G = \left\{ d\varepsilon_{xx}^0 + \frac{z_k + z_{k-1}}{2} d\kappa_{xx}^0, d\varepsilon_{yy}^0 + \frac{z_k + z_{k-1}}{2} d\kappa_{yy}^0, 2d\varepsilon_{xy}^0 + (z_k + z_{k-1}) d\kappa_{xy}^0 \right\}^T. \tag{36}$$

z_k and z_{k-1} are the z coordinates of the top and bottom surfaces of the lamina. These stresses can be transformed into the local coordinates through

$$\{d\sigma\}_k = ([T]_s^T)_k \{d\sigma\}_k^G \tag{37}$$

where another coordinate transformation matrix, $[T]_s$, is defined as

$$[T_s] = \begin{bmatrix} l_1^2 & l_2^2 & l_1 l_2 \\ m_1^2 & m_2^2 & m_1 m_2 \\ 2l_1 m_1 & 2l_2 m_2 & l_1 m_2 + l_2 m_1 \end{bmatrix} \tag{38}$$

Substituting (37) into the right-hand sides of Eqs. (19a) and (19b), the averaged stress increments in the fiber and matrix phases of this lamina can be calculated. It is thus only necessary to determine the middle surface strains and curvature increments, which can be achieved using the classical lamination theory, giving [61]

$$\begin{Bmatrix} dN_{xx} \\ dN_{yy} \\ dN_{xy} \\ dM_{xx} \\ dM_{yy} \\ dM_{xy} \end{Bmatrix} = \begin{bmatrix} Q_{11}^I & Q_{12}^I & Q_{16}^I & Q_{11}^{II} & Q_{12}^{II} & Q_{16}^{II} \\ Q_{12}^I & Q_{22}^I & Q_{26}^I & Q_{12}^{II} & Q_{22}^{II} & Q_{26}^{II} \\ Q_{16}^I & Q_{26}^I & Q_{66}^I & Q_{16}^{II} & Q_{26}^{II} & Q_{66}^{II} \\ Q_{11}^{II} & Q_{12}^{II} & Q_{16}^{II} & Q_{11}^{III} & Q_{12}^{III} & Q_{16}^{III} \\ Q_{12}^{II} & Q_{22}^{II} & Q_{26}^{II} & Q_{12}^{III} & Q_{22}^{III} & Q_{26}^{III} \\ Q_{16}^{II} & Q_{26}^{II} & Q_{66}^{II} & Q_{16}^{III} & Q_{26}^{III} & Q_{66}^{III} \end{bmatrix} \times \begin{Bmatrix} d\varepsilon_{xx}^0 \\ d\varepsilon_{yy}^0 \\ 2d\varepsilon_{xy}^0 \\ d\kappa_{xx}^0 \\ d\kappa_{yy}^0 \\ 2d\kappa_{xy}^0 \end{Bmatrix}, \tag{39}$$

$$Q_{ij}^I = \sum_{k=1}^{N} (C_{ij}^G)_k (z_k - z_{k-1}),$$

$$Q_{ij}^{II} = \frac{1}{2} \sum_{k=1}^{N} (C_{ij}^G)_k (z_k^2 - z_{k-1}^2), \tag{40}$$

$$Q_{ij}^{III} = \frac{1}{3} \sum_{k=1}^{N} (C_{ij}^G)_k (z_k^3 - z_{k-1}^3)$$

where N is the total number of lamina plies in the laminate. $(C_{ij}^G)_k$ are the stiffness elements of the kth lamina in the global coordinate system, see Eq. (33). In Eq. (39), dN_{xx}, dN_{yy}, dN_{xy}, dM_{xx}, dM_{yy}, and dM_{xy} are the overall incremental

Table 8
Material properties of a graphite/epoxy composite ($V_f = 0.7$) under tensile fatigue: retrieved constituent fatigue properties ($R = 0.1$ and $\omega = 18$ Hz)

	Cyclic number, N			
	10^3	10^4	10^5	10^6
σ_u^f (MPa)	1880	1780	1683	1586
σ_u^m (MPa)	26.4	24.8	23.2	21.8
σ_Y^m (MPa)	18	17	15	14
E_T^m (GPa)	1.8	1.8	1.8	1.8

Table 9
Retrieved constituent fatigue properties of a glass/epoxy composite under off-axial fatigue loads ($E^f = 73$ GPa, $\nu^f = 0.22$, $E^m = 3.45$ GPa, $\nu^m = 0.35$, $V_f = 0.6$, $R = 0.1$, and $\omega = 19$ Hz)

	Cyclic number, N					
	0	10^2	10^3	10^4	10^5	10^6
σ_u^f (MPa)	2055	1460	1235	1013	790	570
σ_u^m (MPa)	18.6	19.5	18	16.5	15	13.4
σ_Y^m (MPa)	13	13	13	13	13	12
E_T^m (GPa)	0.21	0.21	0.21	0.21	0.21	0.21

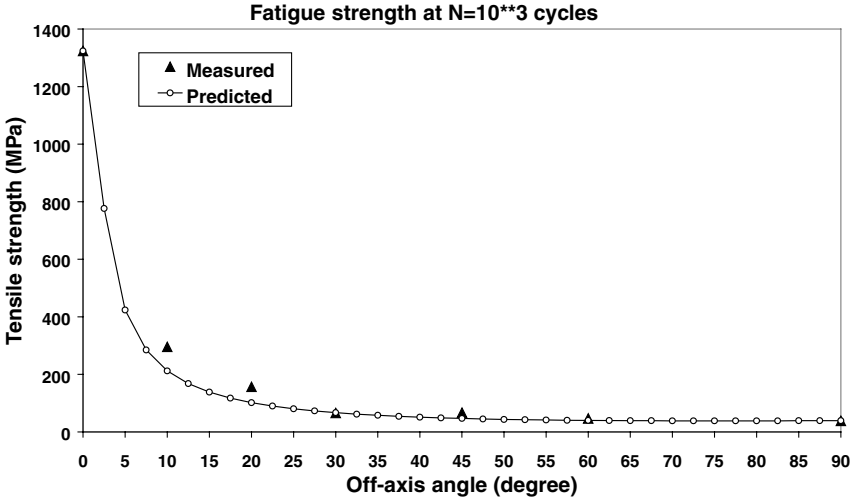

Fig. 7. Comparison between measured [60] and predicted off-axis fatigue strengths of a UD graphite/epoxy composite at $N = 10^3$. The material parameters used are given in Table 5.

in-plane forces and moments per unit length exerted on the laminate, respectively. Suppose that the total applied in-plane stresses are $(\sigma^0_{xx}, \sigma^0_{yy}, \sigma^0_{xy})$. The incremental in-plane forces and moments are defined as

$$\mathrm{d}N_{xx} = \int_{-h/2}^{h/2} (\mathrm{d}\sigma^0_{xx})\,\mathrm{d}z, \qquad \mathrm{d}N_{yy} = \int_{-h/2}^{h/2} (\mathrm{d}\sigma^0_{yy})\,\mathrm{d}z,$$
$$\mathrm{d}N_{xy} = \int_{-h/2}^{h/2} (\mathrm{d}\sigma^0_{xy})\,\mathrm{d}z, \tag{41a}$$

$$\mathrm{d}M_{xx} = \int_{-h/2}^{h/2} (\mathrm{d}\sigma^0_{xx})z\,\mathrm{d}z, \qquad \mathrm{d}M_{yy} = \int_{-h/2}^{h/2} (\mathrm{d}\sigma^0_{yy})z\,\mathrm{d}z,$$
$$\mathrm{d}M_{xy} = \int_{-h/2}^{h/2} (\mathrm{d}\sigma^0_{xy})z\,\mathrm{d}z \tag{41b}$$

where $h = \sum_{k=1}^{N} (z_k - z_{k-1})$ is the whole thickness of the laminate. In all the laminates considered subsequently, each lamina in the laminates will assume a same thickness.

4.1.2. Post-failure analysis

It is evident that different ply in the laminate is subjected to a different load share. Therefore, some lamina ply must have failed first before others. As soon as one ply fails, its contribution to the overall instantaneous stiffness matrix of the laminate must be reduced. Various reduction strategies have been proposed in the literature [62,63]. Here, we adopt a total reduction strategy, which is somewhat similar to that used by Chiu [64]. Once the k_0^{th} lamina ply has

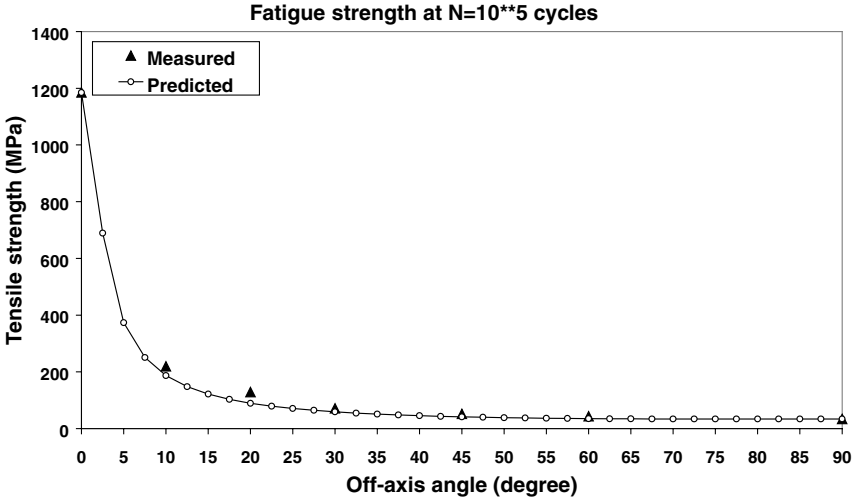

Fig. 8. Comparison between measured [60] and predicted off-axis fatigue strengths of a UD graphite/epoxy composite at $N = 10^5$.

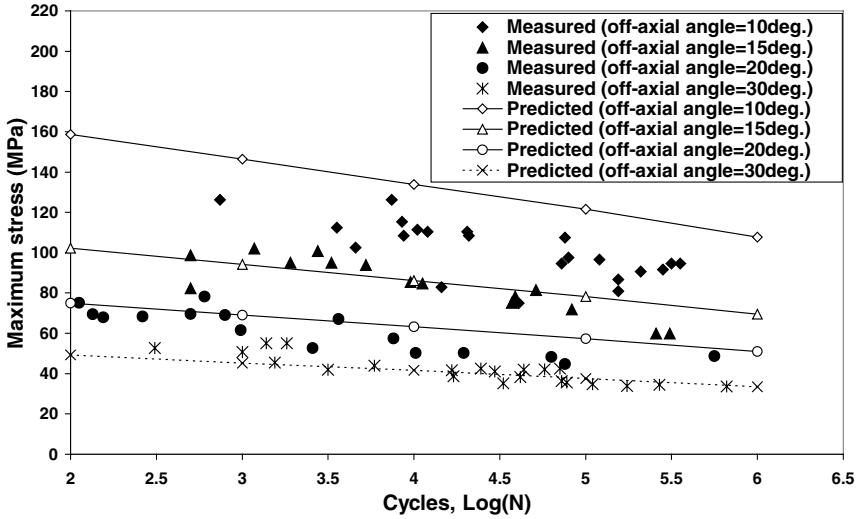

Fig. 9. Comparison between measured [56] and predicted off-axial S–N data of a glass/epoxy composite with off-axial angles of 10, 15, 20, and 30°. The material parameters used are given in Table 6.

failed the stiffness elements in Eq. (39) are redefined as

$$Q_{ij}^{\mathrm{I}} = \sum_{k=1,k\neq k_0}^{N} (C_{ij}^{\mathrm{G}})_k (z_k - z_{k-1}),$$

$$Q_{ij}^{\mathrm{II}} = \frac{1}{2} \sum_{k=1,k\neq k_0}^{N} (C_{ij}^{\mathrm{G}})_k (z_k^2 - z_{k-1}^2), \tag{42}$$

$$Q_{ij}^{\mathrm{III}} = \frac{1}{3} \sum_{k=1,k\neq k_0}^{N} (C_{ij}^{\mathrm{G}})_k (z_k^3 - z_{k-1}^3).$$

Note that the incremental forces and moments are determined using the same formulae, Eqs. (41a) and (41b).

The stiffness reduction, as given by Eq. (42), must be continued until the last-ply has failed, if the laminate is only subjected to an in-plane load. Then, the composite ultimate strength results. If, however, the laminate is involved with a flexural load, the stiffness reduction must be performed more carefully. For example, let the laminate be subjected to only a bending load. The above stiffness reduction process should be stopped before reaching the last or the second last ply failure [42,43]. This is because under the bending condition, the middle plane strain increments, $\mathrm{d}\varepsilon_{xx}^0$, etc. are negligibly small. The remaining bending curvature will have very small, if not zero, stress contribution to the last ply failure or the last two-ply failures, according to Eqs. (35) and (36). For instance, if the laminate consists of odd-number (e.g. 5, 7, 9,…) of plies each of which has the same global property and the same thickness, the central ply will not carry any load no matter how much a pure bending will be applied to the laminate, according to Eqs. (35) and (36). Thus, the last ply will not fail at all, but the deflection (curvature) can be increased unlimitedly. In bending tests of some laminated beams, we have observed that the central ply/plies of the beams cannot be forced to failure due to the limitation of the testing apparatus to excessive beam deflections [42,43]. This is consistent with our theory.

Therefore, if a flexural load is involved, an additional critical deflection/curvature condition has to be employed in order that the ultimate strength of the laminate can be determined [42,43]. However, only in-plane loads will be concerned in the present paper.

4.1.3. Thermal analysis [28,29]

Due to stacking constraint, each lamina in the laminate may be still subjected to nonzero thermal stress components even though no overall load is applied to the laminate. This is because each lamina may have different global coefficients of thermal expansion (although the local ones may be the same).

For the kth lamina, the thermal stress and strain increments in the global coordinate system satisfy [see Eq. (25c)]

$$\{\mathrm{d}\sigma\}_k^{\mathrm{G,(T)}} = [C]_k^{\mathrm{G}} \{\mathrm{d}\varepsilon\}_k^{\mathrm{G,(T)}} - \{\beta\}_k^{\mathrm{G}} \mathrm{d}T \tag{43a}$$

where

$$\{\beta\}_k^{\mathrm{G}} = \{(\beta_1)_k^{\mathrm{G}}, (\beta_2)_k^{\mathrm{G}}, (\beta_3)_k^{\mathrm{G}}\}^{\mathrm{T}} = ([T]_{\mathrm{c}})_k ([S]_k)^{-1} \{\alpha\}_k. \tag{43b}$$

On the other hand, the thermal stress increments applied on the kth lamina in its local coordinate system are obtained from Eq. (37). These stress increments must be substituted into the right-hand sides of Eqs. (26a) and (26b), rather than Eqs. (19a) and (19b), to determine the thermal stress increments in the constituent fiber and matrix materials. Note that the thermal strain

Table 10
Constituent properties of T300/5208 laminates ($V_f = 0.664$) used for inelastic response analysis: elastic and strength parameters ($X = 1619$ MPa, $X' = 900$ MPa, $Y = 49$ MPa, $S = 76$ MPa)

	E_{11} (GPa)	E_{22} (GPa)	G_{12} (GPa)	ν_{12}	σ_u (MPa)	$\sigma_{u,c}$ (MPa)
Fiber[a]	235	15	15	0.25	2417	1342
Matrix[a]	4.2	4.2	1.57	0.34	42	104

[a] Elastic properties were taken from Ref. [50].

increments, $\{d\varepsilon\}_k^{G,(T)}$, in (43a) are defined as

$$\{d\varepsilon\}_k^{G,(T)} = \left\{ d\varepsilon_{xx}^{0,(T)} + \frac{z_k + z_{k-1}}{2} d\kappa_{xx}^{0,(T)}, d\varepsilon_{yy}^{0,(T)} + \frac{z_k + z_{k-1}}{2} d\kappa_{yy}^{0,(T)}, 2d\varepsilon_{xy}^{0,(T)} + (z_k + z_{k-1}) d\kappa_{xy}^{0,(T)} \right\}^T \quad (44)$$

where the middle surface strain and curvature increments due to the temperature variation are obtained from

$$\begin{Bmatrix} d\Omega_1^I \\ d\Omega_2^I \\ d\Omega_3^I \\ d\Omega_1^{II} \\ d\Omega_2^{II} \\ d\Omega_3^{II} \end{Bmatrix} = \begin{bmatrix} Q_{11}^I & Q_{12}^I & Q_{16}^I & Q_{11}^{II} & Q_{12}^{II} & Q_{16}^{II} \\ Q_{12}^I & Q_{22}^I & Q_{26}^I & Q_{12}^{II} & Q_{22}^{II} & Q_{26}^{II} \\ Q_{16}^I & Q_{26}^I & Q_{66}^I & Q_{16}^{II} & Q_{26}^{II} & Q_{66}^{II} \\ Q_{11}^{II} & Q_{12}^{II} & Q_{16}^{II} & Q_{11}^{III} & Q_{12}^{III} & Q_{16}^{III} \\ Q_{12}^{II} & Q_{22}^{II} & Q_{26}^{II} & Q_{12}^{III} & Q_{22}^{III} & Q_{26}^{III} \\ Q_{16}^{II} & Q_{26}^{II} & Q_{66}^{II} & Q_{16}^{III} & Q_{26}^{III} & Q_{66}^{III} \end{bmatrix} \times \begin{Bmatrix} d\varepsilon_{xx}^{0,(T)} \\ d\varepsilon_{yy}^{0,(T)} \\ 2d\varepsilon_{xy}^{0,(T)} \\ d\kappa_{xx}^{0,(T)} \\ d\kappa_{yy}^{0,(T)} \\ 2d\kappa_{xy}^{0,(T)} \end{Bmatrix}, \quad (45)$$

$$d\Omega_i^I = \sum_{k=1}^{N} (\beta_i)_k^G (z_k - z_{k-1}) dT, \qquad d\Omega_i^{II} = \frac{1}{2} \sum_{k=1}^{N} (\beta_i)_k^G (z_k^2 - z_{k-1}^2) dT. \quad (46)$$

4.2. Inelastic response [27]

A number of laminates made using the same graphite/epoxy (T300/5208) UD laminae but placed in different configurations were experimentally investigated by Sendeckyi et al. [65] to obtain their whole stress–strain curves under a longitudinal (x-directional) load condition. The laminae had a nominal fiber volume fraction of $V_f = 0.664$ [65]. The constituent elastic properties together with lamina longitudinal tensile and compressive strengths, X and X', were taken from the literature [50], see also Table 1. No thermal residual stress was assumed for these composites, since no related information was given [65]. The matrix tensile stress–strain curve was retrieved using the lamina in-plane shear stress–strain data, because these data are least influenced by any possible residual thermal stress. The retrieval was performed in such a way that by only adjusting plastic parameters, σ_Y^m and E_T^m, at each load level, the predicted and measured in-plane shear stress–strain curves were in close agreement. The retrieved tensile stress–strain curve was then expressed as a combination of 10 linear segments. A further assumption made was that the matrix had a same stress–strain curve at compression as that at tension. The fiber tensile and compressive strengths were then backed out from X and X', respectively. However, the matrix tensile strength, 36 MPa, retrieved from the lamina transverse tensile strength, Y, was different from the matrix tensile strength, 48 MPa, retrieved from the lamina in-plane shear strength, S. Thus, a simple average was used to define the matrix tensile strength, giving 42 MPa. Finally, the matrix compressive strength was backed out using the ultimate strength of the $[\pm 30]_{2S}$ laminate under a uniaxial load (along 0° direction), because at such load condition the matrix material in the $[\pm 30]_{2S}$ laminate is subjected to essentially compressive stresses. The retrieved constituent properties are summarized in Tables 10 and 11. Using these parameters, the uniaxial stress–strain curves up to final failure of a number of laminates having different stacking arrangements were simulated [27], and some of them are plotted in Figs. 10–13. Good agreement has been found. Additional information is present in Ref. [27].

4.3. Thermal–mechanical strength [28]

Four metal matrix laminates made from the same silicon-carbide fibers (SCS-6) and Ti-15-3 matrix, with a same fiber volume fraction of $V_f = 0.34$, but in different lay-ups were analyzed. Measured uniaxial (in x-direction) tensile

Table 11
Constituent properties of T300/5208 laminates ($V_f = 0.664$) used for inelastic response analysis: plastic parameters of 5208 epoxy matrix

	i									
	1	2	3	4	5	6	7	8	9	10
$(\sigma_Y^m)_i$ (MPa)	28.0	34.8	42.2	49.4	56.4	63.0	69.1	74.8	80.3	83.0
$(E_T^m)_i$ (GPa)	4.20	3.30	3.07	2.63	2.22	1.81	1.45	1.20	0.99	0.42

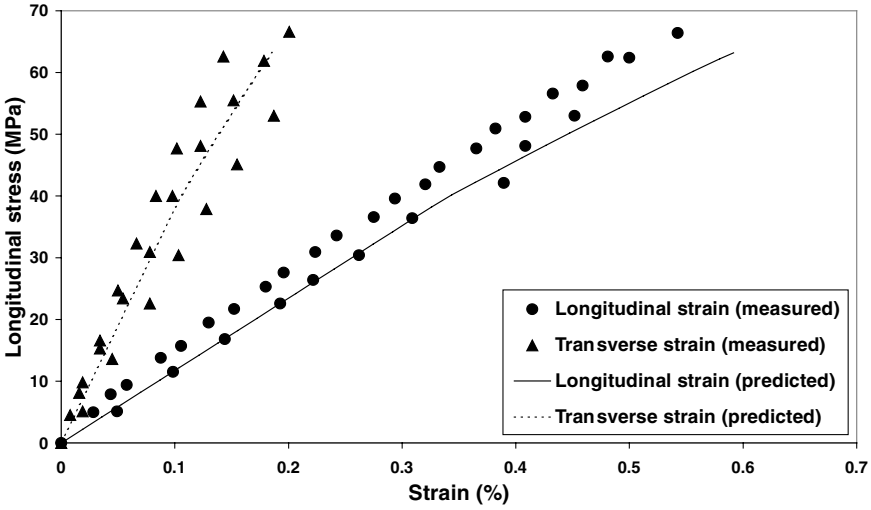

Fig. 10. Longitudinal stress versus longitudinal and transverse strains for T300/5208 $[\pm 60^\circ]_{2S}$ laminate. The material parameters used are given in Table 7, whereas experimental data were taken from Ref. [65].

strengths of these laminates at two or three different temperatures were reported in Ref. [66]. The laminate lay ups as well as the measured laminate tensile strengths at different temperatures are summarized in Table 12, in which the 0°-direction parallels to the global *x*-coordinate. According to Ref. [66], the laminates assumed a stress-free processing temperature of 815°C. Therefore, residual thermal stresses were firstly generated in the constituent fiber and matrix materials when the laminates were cooled down from 815°C to room temperature before applying subsequent thermal and mechanical loads. The SCS-6 fiber was considered as isotropic and linearly elastic until rupture [66], whereas the Ti-15-3 matrix as isotropic and bilinearly elastic–plastic. The thermal–mechanical properties of them, obtained from Refs. [52,67] whenever possibly, are given in Tables 13 and 14, where schemes in determining the remaining constituent parameters are noted. Using these parameters, the laminate final failure strengths at different temperatures were estimated, and are summarized in Table 12. The predictions and the experiments are in reasonable agreement.

4.4. Failure envelope [20,29]

One important feature of the Bridging Model is its simplicity. The model can be easily used to estimate the ultimate failure strength of fibrous composites under any multi-axial stress condition. Let us illustrate this by considering two glass/epoxy laminates subjected to combined bi-axial stress states. The E-glass fiber reinforcement was Silenka 051L, 1200 tex, and the epoxy resin system was Ciba-Geigy MY750/HY917/DY063. All required constituent properties and the properties of a unidirectional lamina made from the same constituents were measured independently [50], and,

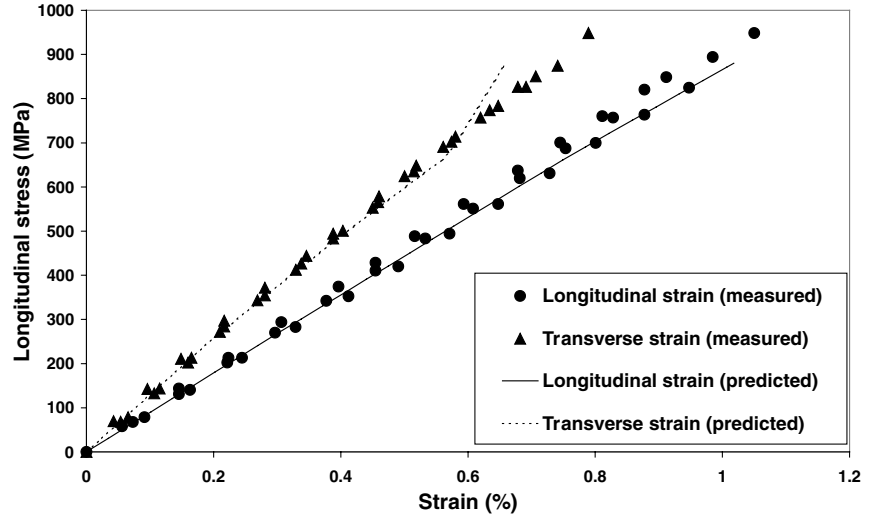

Fig. 11. Longitudinal stress versus longitudinal and transverse strains for T300/5208 $[0^\circ/\pm 45^\circ/0^\circ]_S$ laminate.

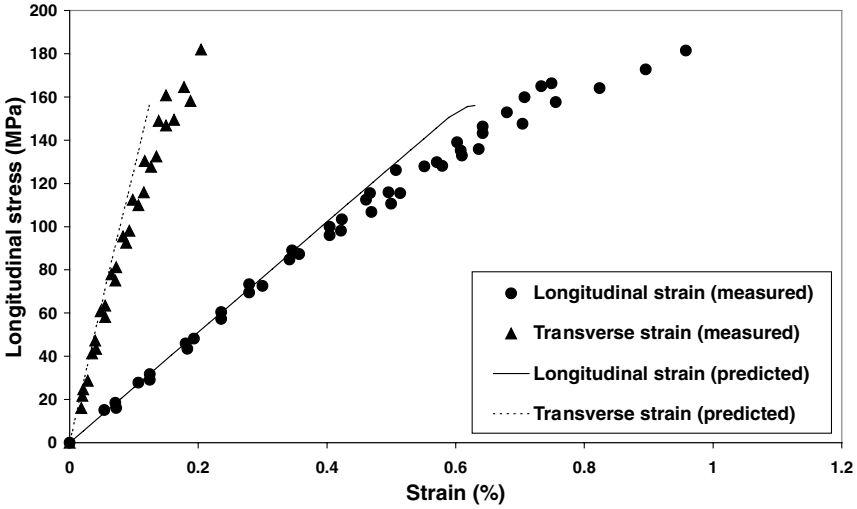

Fig. 12. Longitudinal stress versus longitudinal and transverse strains for T300/5208 $[90°/\pm45°/90°]_S$ laminate.

except for the matrix plastic parameters, are summarized in Table 15 (see also Table 1). In their original data report, Soden et al. [50] only gave the ultimate tensile stress and strain of the epoxy matrix, 80 MPa and 5%. Choosing a typical yield strength of $\sigma_Y^m = 50$ MPa, the matrix hardening modulus was found to be 0.85 GPa, both of which are also listed in Table 15. Using these independent properties, the predicted strength envelopes based on the present theory and on Tsai–Wu's theory [47] for the two angle-ply laminates, $[\pm45°]_s$ and $[\pm55°]_s$, are shown in Figs. 14 and 15. Experimental data reported by Soden et al. [68] are also shown in the figures. It can be seen from the figures that the bridging model predictions are grossly more accurate than the predictions made using Tsai–Wu's theory. It is also noted that the bridging model predictions were based on independent constituent properties whereas the predictions from Tsai–Wu's theory were based on the material parameters measured from the composite. If some overall properties of the composite are used to calibrate some constituent parameters for the bridging model, an improved prediction can be expected. One such an example is shown in Fig. 14, in which the bridging model prediction using a lower matrix compressive strength (without changing any other parameter) gave even better correlation with the experiments. Other more information on bridging model predictions for the 14 multidirectional laminates [50] subjected to biaxial loads has been reported in Ref. [29].

4.5. Life prediction [31]

Rotem and Hashin [69] experimentally measured *S–N* data of angle ply Glass/Epoxy laminates, $[\pm\theta]_{2s}$, with $\theta =$ 30, 35, 41, 45, 49, 55, and 60°. The laminates were subjected to tensile fatigue unixaially along the 0° (*x*-) direction, with a stress ratio of $R = 0.1$ and cyclic frequency $\omega = 19$ or 1.8 cps. Both stress and strain controls were used during

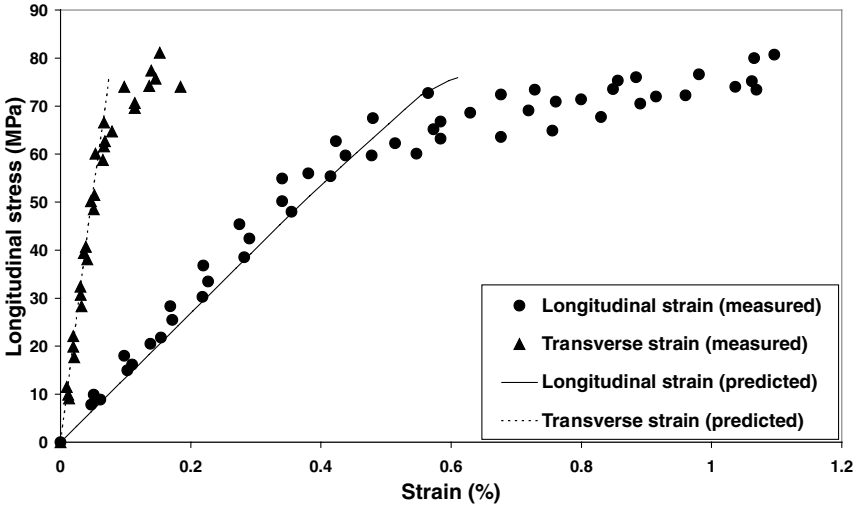

Fig. 13. Longitudinal stress versus longitudinal and transverse strains for T300/5208 $[90°/\pm60°/90°]_S$ laminate.

Table 12
Measured and predicted total tensile strengths of SCS-6/Ti-15-3 composite laminates under uniaxial load ($V_f = 0.34$ and each ply being of same thickness)

Lay-up	Temperature	Measured [66] (MPa)	Predicted (MPa)
$[0]_8$	RT[a]	1336–1517	1425
	427°C	1365–1387	1249
	650°C	948	949
$[0/90]_s$	RT	945–1060	1046.5
	650°C	548	518
$[0_2/\pm45]_s$	RT	1069	1282.1
	650°C	554	792.4
$[0/\pm45/90]_s$	RT	752	994.9
	650°C	421	624.4

[a] RT = room temperature, taken as 25°C.

their tests. From measured lamina behaviors, the elastic properties of the constituents were retrieved (using Eq. (11)), and were assumed unchanged during the cyclic loading. Because a tensile fatigue applied to the $[\pm\theta]_{2s}$ laminate can hardly generate any compressive failure to the fiber material, the fiber compressive strength data were immaterial for the present prediction. The fiber tensile fatigue data were taken from those given in Table 9, whereas the matrix tensile and compressive S–N parameters were back calculated using measured overall S–N data (which were defined similarly as those in Table 6) of the $[\pm60°]_{2s}$ and $[\pm30°]_{2s}$ laminates, given in Table 16. This is because under the uniaxial tensile load condition the matrix in the $[\pm60°]_{2s}$ or $[\pm30°]_{2s}$ laminate is essentially subjected to tension or compression. The constituent fatigue properties are summarized in Table 17, whereas a detailed procedure for the retrieval of the matrix fatigue data is described below.

As the measured stress–strain curves of the composites under static tensile load condition displayed nonlinear behavior [69], the matrix used could not be considered as linearly elastic until rupture. Instead, it was assumed to be bilinearly elastic–plastic in the retrieval. The matrix tensile strength at a given cycle number was specified as the maximum normal stress generated in the matrix of the $[\pm60°]_{2s}$ laminate when it was subjected to the corresponding ultimate tensile load. For example, when the $[\pm60°]_{2s}$ laminate was subjected to the uniaxial tensile stress of 53.6 MPa, which is the fatigue strength of the composite at the cycle number of $N = 0$ (Table 16), the maximum normal stress in the matrix was found to be 35 MPa, which was taken as the matrix tensile strength corresponding to the cycle number of $N = 0$. Meanwhile, the plastic parameters (yield strength and hardening modulus) of the matrix were determined by trial-and-error due to no other information being available, but in such a way that the predicted failure strain of the $[\pm60°]_{2s}$ laminate was as close to the measured value as possible. On the other hand, the predicted unidirectional tensile strength of the lamina based on the so-defined matrix parameters and the other given constituent properties must be equal to the measured strength of the lamina. For example, with the constituent properties of $\sigma_u^f = 2055$ MPa, $\sigma_u^m = 35$ MPa, $\sigma_Y^m = 16$ MPa, and $E_T^m = 0.86$ GPa and a fiber volume fraction of $V_f = 0.60$, the predicted longitudinal strength of the resulting unidirectional lamina is 1247 MPa, which is equal to the measured value at $N = 0$ [56], whereas the predicted ultimate strain of the $[\pm60°]_{2s}$ laminate is 0.8762%, higher than the measured strain, 0.4022% [69]. However, if we take $E_T^m = 2.46$ GPa, the predicted longitudinal strength is 577 MPa, which is incorrect, although the predicted laminate ultimate strain has been improved to 0.4532%. Thus, the matrix plastic and tensile strength parameters at $N = 0$ were chosen as $\sigma_Y^m = 16$ MPa, $E_T^m = 0.86$ GPa, and $\sigma_u^m = 35$ MPa. These plastic parameters were kept unchanged for all the subsequent cycle numbers unless the corresponding longitudinal load was unable to apply to the unidirectional lamina. In such cases ($N = 10^5$ and $N = 10^6$), the matrix yield strengths were adjusted accordingly. For example, with $\sigma_Y^m = 16$ MPa, $E_T^m = 0.86$ GPa, $\sigma_u^m = 21$ MPa, and $\sigma_u^f = 790$ MPa, the predicted longitudinal strength of the unidirectional lamina was lower than 480 MPa, which is the longitudinal tensile strength of the unidirectional lamina at $N = 10^5$ [56]. Thus, the yield strength was adjusted to 15.5 MPa (Table 17), with which the predicted lamina longitudinal strength is 480 MPa. The retrieved matrix tensile strengths and plastic parameters at cycle numbers of $N = 0$ to $N = 10^6$ are listed in Table 17.

Under the assumption that the matrix plasticity at compression was the same as that at tension, the compressive strengths of the matrix at the chosen cycle numbers were back calculated straightforwardly: by applying the uniaxial loads at the respective numbers to the $[\pm30°]_{2s}$ laminate, the maximum compressive stresses ($-\sigma^3$) in the matrix were taken as the matrix compressive strengths at the corresponding cycle numbers.

Using the constituent properties given in Table 17, the predicted S–N curves of angle ply laminates with $\theta = 35$, 41, 45, 49, and 55° are plotted in Figs. 16–20, respectively. For comparison, the measured data by Rotem and Hashin [69] are also shown in the corresponding figures. It is seen

Table 13
Thermoelastic properties of the SCS-6 fiber [67]

T (°C)	E_f (GPa)	ν_f	σ_u^f (MPa)	α_f ($\times 10^{-6}$/°C)
25	393	0.25	2600[a]	3.564
93	390	0.25	2576[b]	3.660
204	386	0.25	2537[b]	3.618
316	382	0.25	2498[b]	3.638
427	378	0.25	2458[b]	3.687
538	374	0.25	2419[b]	3.752
650	370	0.25	2380[a]	3.826
760	365	0.25	2341[c]	3.903
871	361	0.25	2302[c]	3.980
1093	354	0.25	2224[c]	4.103

[a] Retrieved using the tensile strength of $[0°]_8$ laminate.
[b] Interpolated.
[c] Extrapolated.

Table 14
Material properties of the Ti-15-3 matrix [67]

T (°C)	E^m (GPa)	σ_Y^m (MPa)	E_T^m (GPa)	ν^m	σ_u^m (MPa)	α_m ($\times 10^{-6}$/°C)
25	83.6	763	3.32	0.36	848[a]	8.48
315	80.4	645[b]	3.54[b]	0.36	719[c]	9.16
482	72.2	577	3.67	0.36	645[c]	9.71
538	67.8	447	2.69	0.36	500 [52]	9.89
566	64.4	287	2.39	0.36	321[c]	9.98
650	53.0	198	1.12	0.36	222[c]	10.26
900	25.0	20[b]	0.8[b]	0.36	22[c]	10.50

[a] Retrieved using the tensile strength of $[0/90]_{2s}$ laminate.
[b] Interpolation/extrapolation value.
[c] Determined according to: $\sigma_u^m(T) = \alpha(T)\sigma_Y^m(T)$, $\alpha(T) = \alpha_1 + [(T - 25)/(538 - 25)](\alpha_2 - \alpha_1)$, $\alpha_1 = 848/763 = 1.1114$ and $\alpha_2 = 500/447 = 1.1186$.

that correlation between all the predictions and the experiments is satisfactorily high.

Finally, it deserves special mentioning that the present prediction can also display clearly the averaged interlaminar stress in the laminate, i.e. the stress component in the thickness direction. This stress is critical to the laminate delamination. The present prediction indicated that under the tensile fatigue load, the two in-plane principal stresses, i.e. σ_{max}^m and σ_{min}^m, in the matrix material of the $[\pm\theta]_{2s}$ laminate have a negative averaged value (i.e. $\sigma_{max}^m + \sigma_{min}^m < 0$) when $8° < \theta < 44°$. The σ_{min}^m attains a critical value when $16° < \theta \leq 39°$. Out of that range, i.e. when $\theta \leq 8°$ or $\theta \geq 44°$, the sum of the two in-plane principal stresses is positive. According to the classical lamination theory, the out-of-plane strain components are zero. This means that a positive stress component will be generated in the matrix in the thickness direction, due to Poisson's ratio effect, when $8° < \theta < 44°$, and will attain the largest when $16° < \theta \leq 39°$. Such a stress component is the source to initiate the laminate delamination. Thus, an angle-plied laminate made from the current glass/epoxy system subjected to a uniaxial tensile (fatigue) load may generate delamination when $8° < \theta < 44°$, and most probably when $16° < \theta \leq 39°$. On the contrary, no delamination can occur when $\theta \leq 8°$ or $\theta \geq 44°$. These observations are consistent with Rotem and Hashin's experimental evidences [69]. They noticed that the laminate failure was initiated by delamination at edges when $\theta < 45°$ (i.e. for the $[\pm 30°]_s$, $[\pm 35°]_s$, and $[\pm 41°]_s$ laminates), whereas no delamination occurred in the $[\pm\theta]_s$ laminates when $\theta > 45°$.

5. Summary remarks

(1) The bridging parameters, β and α, in Eqs. (7b) and (7c), can be adjusted using measured transverse and in-plane shear moduli of a unidirectional composite, respectively. They have effect on both the predicted elastic properties and the predicted ultimate strength of the composite. It has been found that without changing the predicted elastic modulus significantly, a smaller value in β or α would give a slightly better prediction for an off-axial strength of some composites. If no other information is available, the following recommendations can be considered for these two parameters:

$$\beta = 0.4\text{–}0.45 \qquad \text{and} \qquad \alpha = 0.3\text{–}0.35.$$

It should be pointed out that not too much difference can be experienced when using some other bridging parameters, as indicated in most examples of this paper, in which $\beta = \alpha = 0.5$ have been used.

(2) The power index, q, in Eq. (20b) is an empirical parameter. One example (Fig. 14) in this paper suggested that this parameter should be greater than 2. However, by choosing $q = 3$, only some small difference can be observed between the classical and the generalized maximum normal stress criteria. As such, the simpler classical maximum normal stress criterion should be able to generate reasonably good predictions in most cases. The majority of the results shown in this paper were obtained just based on the classical maximum normal stress criterion.

(3) The matrix plasticity is not very important for lamina strength prediction, as long as the lamina is statically

Table 15
Material properties of a glass/epoxy lamina (Silenka 051L/MY750/HY917/DY063) used for failure envelope prediction ($E_f = 74$ GPa, $\nu_f = 0.2$, $E^m = 3.35$ GPa, $\nu^m = 0.35$, $\sigma_Y^m = 50$ MPa, $E_T^m = 850$ MPa, $E_{11} = 45.6$ GPa, $E_{22} = 16.2$ GPa, $\nu_{12} = 0.278$, $G_{12} = 5.83$ GPa, and $V_f = 0.60$)

	Longitudinal tensile strength (MPa)	Longitudinal compressive strength (MPa)	Transverse tensile strength (MPa)	Transverse compressive strength (MPa)	In-plane shear strength (MPa)
Fiber	2150	1450	–	–	–
Matrix	80	120	–	–	–
Lamina	1280	800	40	145	73

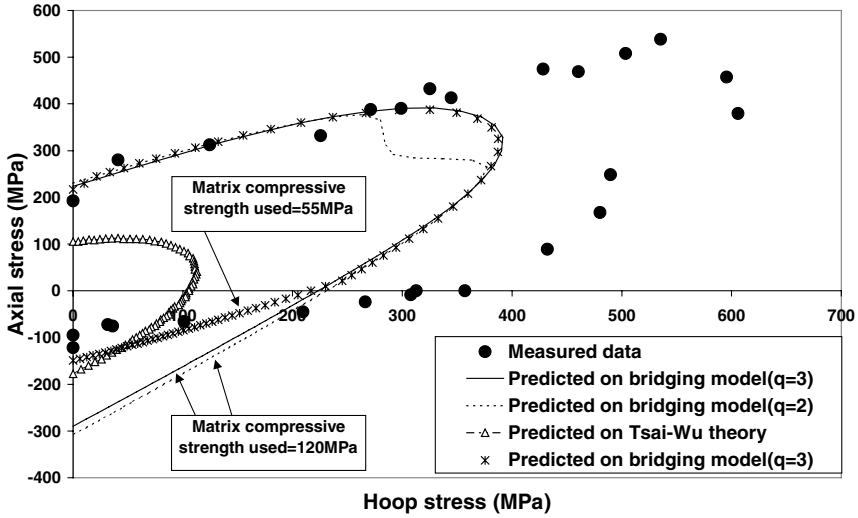

Fig. 14. Predicted and measured [68] failure envelopes of a [±45°] glass/epoxy shell of $V_f = 0.504$, subjected to combined axial and circumferential tensile loads.

determinate (i.e. the stress components applied to the lamina can be determined only using an equilibrium condition) and as long as the fiber fracture controls the longitudinal failure of the composite. Another implicit assumption involved is that the fiber stiffness should be significantly higher than the matrix stiffness. In contrast, the matrix plasticity becomes very important for laminate progressive failure analysis and for its strength prediction. The reason is that an angle-plied lamina in the laminate becomes always statically indeterminate.

(4) The in situ constituent strength parameters, especially the matrix ultimate strength, are crucial to the accurate prediction of the resulting composite strength. This is because the failure of most composites, except for those that carry out a main load component closer to the fiber direction, results from the matrix fracture, based on the bridging model theory. It is noted that this conclusion is valid only when the stiffness and strength of the fibers are significantly higher than those of the matrix. On the other hand, the composite transverse and in-plane shear responses are quite sensitive to the composite fabrication conditions involved. As such, the matrix ultimate strengths (tensile and compressive strengths) should be, whenever possibly, calibrated using overall uniaxial strengths of the composite along some proper directions. If a laminate is going to be accurately analyzed, some laminate strength rather than lamina strength should be used in the calibration. On the contrary, the matrix plastic parameters or stress–strain curves obtained from bulk material tests under both tension and compression can be directly employed in the bridging model simulation.

(5) For most composite examples shown in this paper,

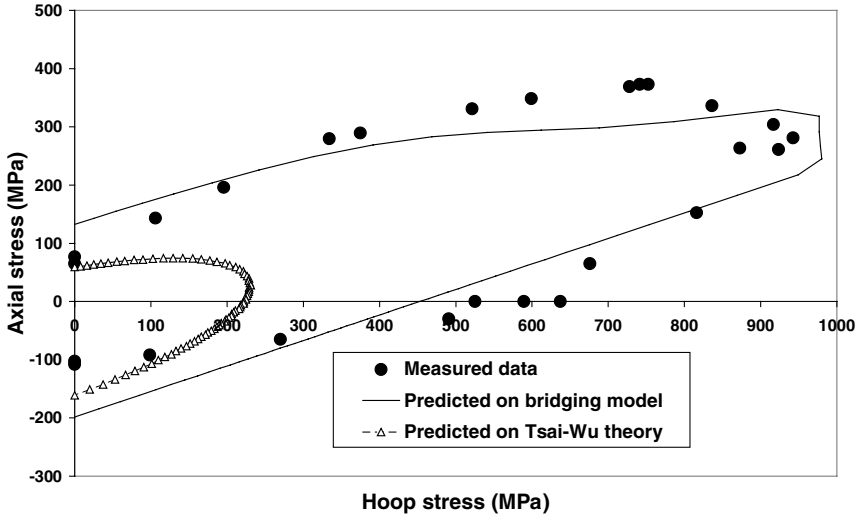

Fig. 15. Predicted and measured [68] failure envelopes of a [±55°] glass/epoxy shell of $V_f = 0.602$, subjected to combined axial and circumferential tensile loads.

Table 16
Measured [69] failure stresses of angle ply laminates (MPa)

Lay up	Cycles to failure, N					
	0	10^2	10^3	10^4	10^5	10^6
± 30°	343.5	343.5[a]	288.6	229.2	169.9	110.5
± 60°	53.6	53.6[b]	48.9	40.6	32.3	24

[a] Linear extrapolation = 347.9.
[b] Linear extrapolation = 57.3.

their constituent matrix materials have been subjected to essentially tensile loads or have been assumed to take the same response (i.e. the same elastic and plastic properties) at compression as that at tension. The latter assumption is seen to be inaccurate in general, and may be attributed to one reason that some parts of the simulation results did not show very high correlation with the corresponding experiments. As can be understood, in reality, most matrix materials, especially polymer matrices, do exhibit different response at compression than that at tension. Therefore, different matrix properties should be employed for a more accurate simulation, depending on whether the matrix material in the composite is subjected to the resulting tension or compression. However, the matrix material in a complex composite such as a multidirectional laminate or a textile fabric reinforced composite is generally subjected to the resulting multiaxial stress-state even though the composite itself is under a simple uniaxial load condition. It is highly possible that some of the matrix stress components are positive (tensile) while the others are negative (compressive). A criterion is thus necessary to indicate whether the material is subjected to essential tension or compression. A straightforward choice for this is to use the three material principal stresses [40,41]: if the sum of these three stresses is negative, the material is understood to be under compression; otherwise, it is under tension. Namely [40,41],

if $(\sigma^1)_m + (\sigma^2)_m + (\sigma^3)_m < 0$, the matrix is under essential compression;
if $(\sigma^1)_m + (\sigma^2)_m + (\sigma^3)_m \geq 0$, the matrix is under essential tension.

Table 17
Retrieved constituent fatigue properties of glass/epoxy laminates used for life prediction ($E^f = 80$ GPa, $\nu^f = 0.25$, $E^m = 4.0$ GPa, $\nu^m = 0.35$, and $V_f = 0.65$)

	Cycles to failure, N					
	0	10^2	10^3	10^4	10^5	10^6
σ_u^f (MPa)	2055	1460	1235	1013	790	570
σ_u^m (MPa)	35.0	35.0	32.0	26.5	21.0	16.0
$\sigma_{u,c}^m$ (MPa)	70.0	70.0	59.0	47.0	34.0	22.0
σ_Y^m (MPa)	16.0	16.0	16.0	16.0	15.5	12.0
E_T^m (GPa)	0.86	0.86	0.86	0.86	0.86	0.86

In the above, $(\sigma^1)_m$, $(\sigma^2)_m$, and $(\sigma^3)_m$ stand for the three principal stresses in the matrix.

(6) When the constituent elastic as well as matrix plastic parameters have been given, the retrieval of only the constituent strengths is performed straightforwardly. By simply applying some uniaxial load to the composite until its ultimate level (i.e. the level which would have caused the composite to fail), the resulting maximum (or equivalent maximum, in Eq. (20)) normal stress in the matrix or the fiber is defined as the ultimate strength of the matrix or the fiber.

(7) The composite theory (i.e. the basic equations (2a)–(2e)) was established at the level of a representative volume element (RVE). By definition, a RVE is the smallest repeating element in the composite. Therefore, it can be a single fiber together with a matrix enclosure, as indicated in Fig. A1. The bridging model has been developed with respect to the RVE: as long as the overall applied load on the RVE is given, the composite internal response can be determined with this model. Different RVEs in the composite (such as a composite structure or component) may sustain different overall loads. An FEM Software package can be used to determine the overall loads on all the elements of the composite, whereas the bridging model is incorporated to determine the internal response and instantaneous stiffness matrix (elemental local stiffness matrix) of an element. Evidently, one Finite Element may contain quite a lot of RVEs, and the analysis becomes more and more accurate when the Finite Element contains less and less RVEs.

6. Conclusions

A recently developed micromechanics model, the Bridging Model, is summarized and reviewed in this paper. The model is so general that it can be applied to essentially any continuous fiber reinforced composite, and yet is so easy to implement that it only involves explicit formulae and requires no iteration especially when the composite is subjected to a planar load condition. Potential applications of the model to estimate various mechanical properties of unidirectional laminae and multidirectional laminates, including thermo-elastic behavior, ultimate strength, inelastic response, strength at elevated temperature, strength envelope, fatigue life and S–N curve, etc. have been demonstrated in this paper. Its powerful applications to textile fabric (knitted, woven, and braided fabrics) reinforced composites will be reviewed in a subsequent paper.

Appendix A

Let V' denote the volume of the representative volume element (RVE) of a UD composite, as shown in Fig. A1. The volumes of the fiber and the matrix in the RVE are V'_f and V'_m, respectively. Suppose that the ith point-wise stress in the RVE is σ_i which may be different at a different point.

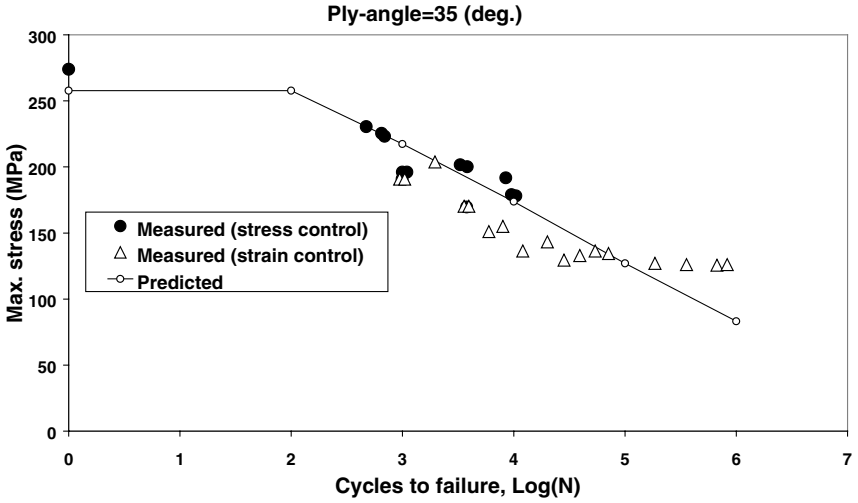

Fig. 16. Predicted and measured [69] *S–N* curves of a glass/epoxy $[\pm 35°]_s$ laminate.

The volume-averaged stress $\bar{\sigma}_i$ of the composite is defined as

$$\overline{\sigma_i} = \frac{1}{V'}\int_{V'} \sigma_i \, dV = \frac{1}{V'}\left[\int_{V'_f} \sigma_i \, dV + \int_{V'_m} \sigma_i \, dV\right]$$
$$= \left(\frac{V'_f}{V'}\right)\left(\frac{1}{V'_f}\int_{V'_f} \sigma_i \, dV\right) + \left(\frac{V'_m}{V'}\right)\left(\frac{1}{V'_m}\int_{V'_m} \sigma_i \, dV\right)$$
$$= V_f\overline{\sigma_i^f} + V_m\overline{\sigma_i^m},$$
$$i = 1, 2, \ldots, 6, \tag{A1}$$

where V_f $(= V'_f/V')$ and V_m $(= V'_m/V')$ are the volume fractions of the fiber and the matrix, respectively, and $\overline{\sigma_i^f}$ and $\overline{\sigma_i^m}$ are the volume-averaged constituent stresses. Similarly, we can derive an identity for volume averaged strains among $\overline{\varepsilon_i}$, $\overline{\varepsilon_i^f}$, and $\overline{\varepsilon_i^m}$. As we are only concerned with volume averaged stresses and strains, the over-bar can be omitted. Thus, Eq. (2a) holds in any case. Further, the constitutive relationship between volume averaged stresses and strains has the same form as that between point-wise stresses and strains, because a compliance matrix is independent of volume averaging. This shows that Eqs. (2c)–(2e) are correct.

Appendix B

Volume averaged stresses and strains in a representative volume element (RVE) of the lamina satisfy (Appendix A)

$$\{d\sigma\} = V_f\{d\sigma^f\} + V_m\{d\sigma^m\} \tag{B1}$$

and

$$\{d\varepsilon_i\} = V_f\{d\varepsilon^f\} + V_m\{d\varepsilon^m\}. \tag{B2}$$

The constitutive equations correlating the averaged stresses

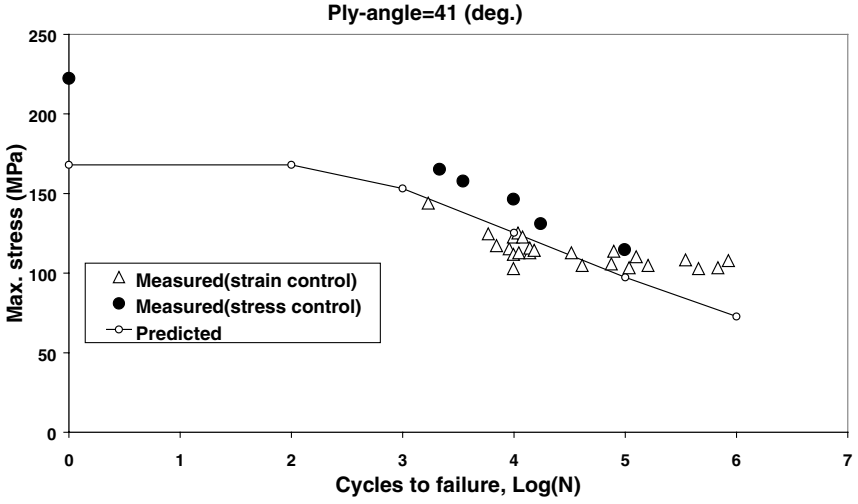

Fig. 17. Predicted and measured [69] *S–N* curves of a glass/epoxy $[\pm 41°]_s$ laminate.

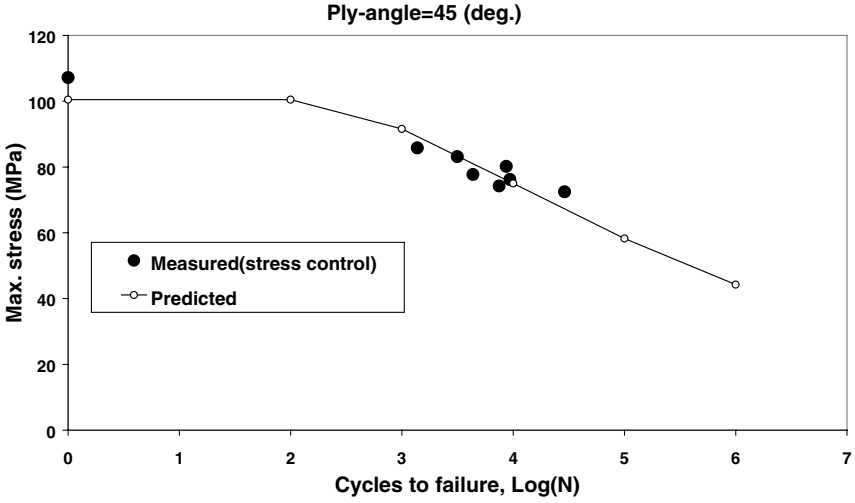

Fig. 18. Predicted and measured [69] S–N curves of a glass/epoxy $[\pm 45^\circ]_s$ laminate.

and strains in different phases of the RVE are expressed as

$$\{d\varepsilon^f\} = [S^f]\{d\sigma^f\}, \tag{B3}$$

$$\{d\varepsilon^m\} = [S^m]\{d\sigma^m\}, \tag{B4}$$

and

$$\{d\varepsilon\} = [S]\{d\sigma\}. \tag{B5}$$

Substituting Eq. (1) into Eq. (B1) and inverting the resulting equations yields Eq. (4a), whereas substituting Eq. (4a) into Eq. (1) gives Eq. (4b). Further, substituting (B3) and (B4) into (B2) and making use of (1), one obtains (B5), or Eq. (3). Let us consider an elastic deformation first. In such a case, the overall compliance matrix of the lamina, Eq. (3), reads

$$[S] = \begin{bmatrix} [S_{ij}]_\sigma & 0 \\ 0 & [S_{ij}]_\tau \end{bmatrix}, \tag{B6a}$$

where

$$[S_{ij}]_\sigma = \begin{bmatrix} 1/E_{11} & -\nu_{12}/E_{11} & -\nu_{12}/E_{11} \\ & 1/E_{22} & -\nu_{23}/E_{22} \\ \text{symmetry} & & 1/E_{22} \end{bmatrix}, \tag{B6b}$$

and

$$[S_{ij}]_\tau = \begin{bmatrix} 1/G_{23} & 0 & 0 \\ & 1/G_{12} & 0 \\ \text{symmetry} & & 1/G_{12} \end{bmatrix}. \tag{B6c}$$

Note that the material parameters E_{22}, G_{23}, and ν_{23} are not all independent but are related by

$$G_{23} = \frac{E_{22}}{2(1+\nu_{23})}. \tag{B7}$$

Therefore, there are only five independent elements in the

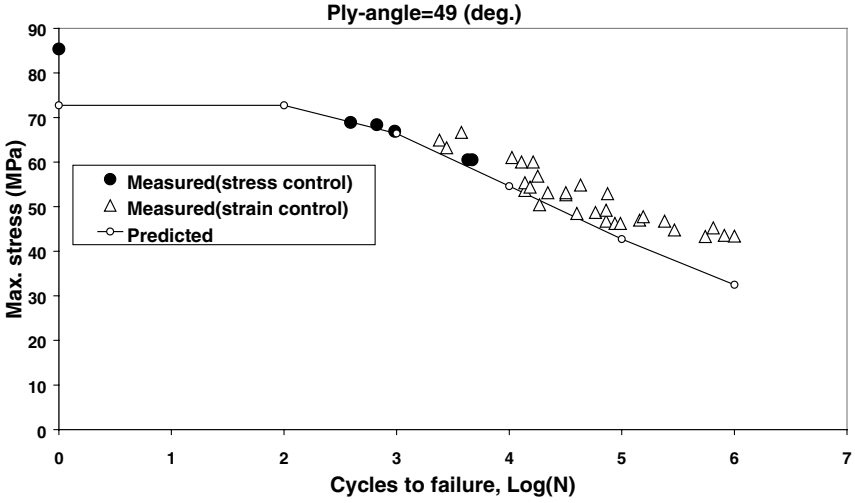

Fig. 19. Predicted and measured [69] S–N curves of a glass/epoxy $[\pm 49^\circ]_s$ laminate.

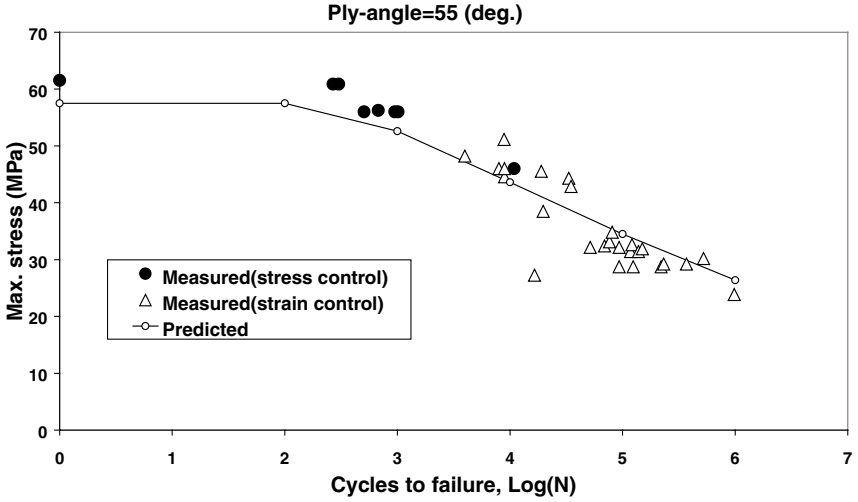

Fig. 20. Predicted and measured [69] S–N curves of a glass/epoxy $[\pm 55^\circ]_s$ laminate.

bridging matrix (6). The other nonzero elements are determined by substituting (6) into (3) and by making the resulting compliance matrix to be symmetric [see Eq. (5)]. Note that the constituent compliance matrices, $[S^f]$ and $[S^m]$, have the same structure as that of $[S]$, Eqs. (B6a)–(B6c). Hence, the most general form of the bridging matrix (in an elastic region) should read

$$[A_{ij}] = \begin{bmatrix} a_{11} & a_{12} & a_{13} & & & \\ a_{21} & a_{22} & a_{23} & & & \\ a_{31} & a_{32} & a_{33} & & & \\ & & & a_{44} & & \\ & & & & a_{55} & \\ \text{remaining zero} & & & & & a_{66} \end{bmatrix}. \tag{B8}$$

As G_{12} is an independent modulus, the bridging element $a_{55} = a_{66}$ must be independent. In light of Eq. (B.), i.e. G_{23} is not independent, the other four independent bridging elements should be among a_{ij}'s where $i \le 3$ and $j \le 3$. We may thus set $a_{21} = a_{31} = 0$, and take a_{11}, a_{22}, a_{33}, and a_{32} to be independent.

Substituting the chosen $[A_{ij}]$ into Eq. (3) and imposing that $S_{ji} = S_{ij}$ for all $i, j = 1, 2, 3$, three algebraic equations are obtained as follows:

$$\alpha_{11}a_{12} + \alpha_{12}a_{13} + \alpha_{13}a_{23} = p_1, \tag{B9a}$$

$$\alpha_{21}a_{12}a_{23} + \alpha_{22}a_{13} + \alpha_{23}a_{23} = p_2, \tag{B9b}$$

$$\alpha_{31}a_{12}a_{23} + \alpha_{32}a_{12} + \alpha_{33}a_{13} + \alpha_{34}a_{23} = p_3. \tag{B9c}$$

In Eqs. (B9a)–(B9c), the parameters α_{ij}'s and p_i's are given by:

$$\alpha_{11} = (V_f + V_m a_{33})(S_{11}^f - S_{11}^m),$$

$$\alpha_{12} = -V_m(S_{11}^f - S_{11}^m)a_{32},$$

$$\alpha_{13} = -V_m(S_{12}^f - S_{12}^m)a_{32},$$

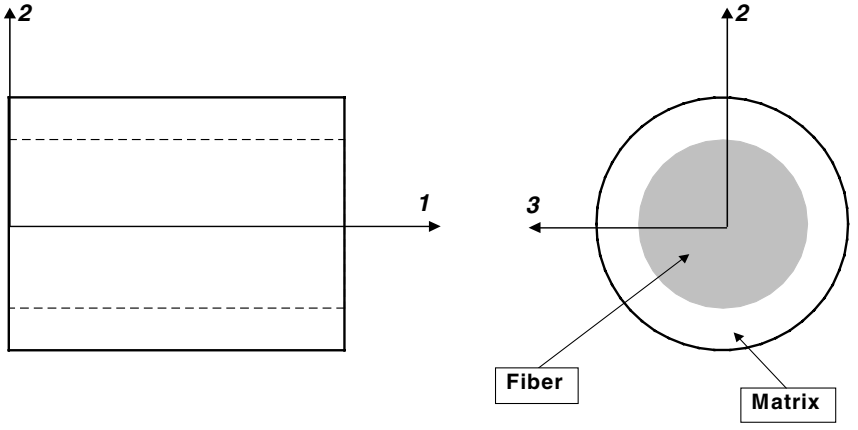

Fig. A1. A representative volume element of a UD composite.

$$\alpha_{21} = V_m(S^f_{11} - S^m_{11}),$$

$$\alpha_{22} = -(V_f + V_m a_{22})(S^f_{11} - S^m_{11}),$$

$$\alpha_{23} = -[(V_f + V_m a_{11})(S^f_{12} - S^m_{12}) - V_m(S^f_{13} - S^m_{13})a_{32}],$$

$$\alpha_{31} = V_m(S^f_{12} - S^m_{12}),$$

$$\alpha_{32} = (V_f + V_m a_{33})(S^f_{31} - S^m_{31}),$$

$$\alpha_{33} = -[(V_f + V_m a_{22})(S^f_{12} - S^m_{12}) + V_m(S^f_{31} - S^m_{31})a_{32}],$$

$$\alpha_{34} = -(V_f + V_m a_{11})(S^f_{22} - S^m_{22}),$$

$$p_1 = (V_f + V_m a_{33})(S^f_{12} - S^m_{12})(a_{11} - a_{22}) - (V_f + V_m a_{11})(S^f_{13} - S^m_{13})a_{32},$$

$$p_2 = (V_f + V_m a_{22})(S^f_{13} - S^m_{13})(a_{33} - a_{11}),$$

$$p_3 = (V_f + V_m a_{11})[(S^f_{23} - S^m_{23})(a_{33} - a_{22}) - (S^f_{33} - S^m_{33})a_{32}].$$

As Eqs. (B9a)–(B9c) are nonlinear, there might exist two sets of solutions to a_{12}, a_{13}, and a_{23}. Choosing a_{12} as the primary variable, two solutions of it are given, respectively, by

$$a^I_{12} = \frac{-b + \sqrt{b^2 - 4ac}}{2a}, \qquad a^{II}_{12} = \frac{-b - \sqrt{b^2 - 4ac}}{2a}, \tag{B10a}$$

where $a = \alpha_{21}\gamma_2$, $b = \alpha_{21}\beta_2 + \alpha_{22}\gamma_1 + \alpha_{23}\gamma_2$, $c = \alpha_{22}\beta_1 + \alpha_{23}\beta_2 - p_2$,

$$\beta_1 = \frac{[\alpha_{13}(p_3/\alpha_{31} - p_2/\alpha_{21}) - p_1(\alpha_{34}/\alpha_{31} - \alpha_{23}/\alpha_{21})]}{\alpha_{13}(\alpha_{33}/\alpha_{31} - \alpha_{22}/\alpha_{21}) - \alpha_{12}(\alpha_{34}/\alpha_{31} - \alpha_{23}/\alpha_{21})}, \tag{B10b}$$

$$\beta_2 = \frac{[p_1(\alpha_{33}/\alpha_{31} - \alpha_{22}/\alpha_{21}) - \alpha_{12}(p_3/\alpha_{31} - p_2/\alpha_{21})]}{\alpha_{13}(\alpha_{33}/\alpha_{31} - \alpha_{22}/\alpha_{21}) - \alpha_{12}(\alpha_{34}/\alpha_{31} - \alpha_{23}/\alpha_{21})}, \tag{B10c}$$

$$\gamma_1 = \frac{[-\alpha_{13}(\alpha_{32}/\alpha_{31}) + \alpha_{11}(\alpha_{34}/\alpha_{31} - \alpha_{23}/\alpha_{21})]}{\alpha_{13}(\alpha_{33}/\alpha_{31} - \alpha_{22}/\alpha_{21}) - \alpha_{12}(\alpha_{34}/\alpha_{31} - \alpha_{23}/\alpha_{21})}, \tag{B10d}$$

$$\gamma_2 = \frac{[\alpha_{12}(\alpha_{32}/\alpha_{31}) - \alpha_{11}(\alpha_{33}/\alpha_{31} - \alpha_{22}/\alpha_{21})]}{\alpha_{13}(\alpha_{33}/\alpha_{31} - \alpha_{22}/\alpha_{21}) - \alpha_{12}(\alpha_{34}/\alpha_{31} - \alpha_{23}/\alpha_{21})}. \tag{B10e}$$

With formulae (B10a)–(B10e), the other two variables are obtained as

$$a_{13} = \beta_1 + \gamma_1 a_{12}, \qquad a_{23} = \beta_2 + \gamma_2 a_{12}. \tag{B10f}$$

The independent elements, a_{11}, a_{22}, a_{33}, and a_{32}, are expected to depend on the elastic properties of the matrix and the fibers, and on the fiber packing geometry (the relative position of the fibers embedded in the matrix, the fiber volume fraction, the fiber cross-sectional shapes, etc.). When the properties of the two materials become the same, the bridging matrix, $[A_{ij}]$, must be identical (of unit matrix). Hence, the general forms of the independent elements are always expressible as the power series of the material properties, i.e.

$$a_{11} = 1 + \beta_{11}(1 - E^m/E^f_{11}) + \cdots, \tag{B11a}$$

$$a_{22} = 1 + \beta_{21}(1 - E^m/E^f_{22}) + \cdots, \tag{B11b}$$

$$a_{32} = \beta_{31}(1 - E^m/E^f_{11}) + \beta_{32}(1 - \nu^m/\nu^f_{12}) + \cdots, \tag{B11c}$$

$$a_{33} = 1 + \beta_{41}(1 - E^m/E^f_{22}) + \cdots, \tag{B11d}$$

$$a_{55} = a_{66} = 1 + \beta_{51}(1 - G^m/G^f_{12}) + \cdots, \tag{B11e}$$

where β_{ij}'s only depend on the fiber packing geometry but are independent of material properties. For clarity, we call β_{ij}'s as bridging parameters.

The most rigorous method to determine the bridging parameters is through experiments. Supposing that the five elastic constants of the composite have been measured, the bridging parameters can be determined using some best approximation, such as the least-squares techniques. However, explicit expressions for them are much more important in application. The most significant feature is that when the bridging parameters are determined using an elastic deformation condition, they remain unchanged during an inelastic deformation. As the composite elasticity theory has already been fairly well established, we may use it to explicitly determine a set of bridging parameters.

Thus, let us imagine that a representative volume element is composed of a concentric cylinder (Fig. A1). Based on this, some rigorous analyses have been done and it was found that [70]:

$$\sigma^m_{12} = a_{66}\sigma^f_{12}, \tag{B12a}$$

where

$$a_{66} = \frac{1}{2}\left(1 + \frac{G^m}{G^f_{12}}\right). \tag{B12b}$$

Comparing (B12b) with (B11e), we see that

$$\beta_{51} = -0.5. \tag{B13}$$

Further, experiments have shown that the overall longitudinal stress of a unidirectional fiber reinforced composite is comparable with the stress of the fiber in the same direction, whereas the overall transverse stress of the composite is comparable with the matrix stress in that direction. It is thus reasonable to assume that the averaged normal stresses between the fiber and the matrix are correlated by

$$\sigma^m_{11} = a_{11}\sigma^f_{11} + a_{12}\sigma^f_{22} + a_{13}\sigma^f_{33}, \tag{B14a}$$

$$\sigma_{22}^{m} = a_{22}\sigma_{22}^{f}, \tag{B14b}$$

$$\sigma_{33}^{m} = a_{33}\sigma_{33}^{f}. \tag{B14c}$$

Because of the axi-symmetry of the concentric cylinder geometry, we may further assume that $a_{33} = a_{22}$. Substituting so defined a_{ij}'s, i.e.

$$a_{21} = a_{31} = a_{23} = a_{32} = 0 \qquad \text{and} \qquad a_{33} = a_{22} \tag{B15}$$

into Eq. (B10), it is found that

$$a_{13} = a_{12} = (S_{12}^{f} - S_{12}^{m})(a_{11} - a_{22})/(S_{11}^{f} - S_{11}^{m}). \tag{B16}$$

Hence, there are only two independent elements, a_{11} and a_{22}, to be defined. Again, substituting (B15) into Eq. (3) and making some manipulation, the longitudinal Young's modulus is obtained as

$$E_{11} = \frac{(V_f + V_m a_{11})}{(V_f S_{11}^{f} + V_m a_{11} S_{11}^{m})}. \tag{B17}$$

It is well known that the rule of mixture approach gives a quite accurate approximation to the composite longitudinal modulus. Supposing that the modulus defined by (B17) is equal to that given by the rule of mixture formula, we get

$$a_{11} = E^{m}/E_{11}^{f} \tag{B18}$$

or

$$\beta_{11} = -1. \tag{B19}$$

It is noted that with this set of a_{ij}'s, the resulting longitudinal Poisson's ratio, ν_{12}, is exactly the same as that given by the rule of mixture formula, i.e. $\nu_{12} = V_f \nu_{12}^{f} + V_m \nu^{m}$.

There remains a_{22}, which defines the transverse modulus E_{22}, to be determined. Many different micro-mechanical formulae have been proposed for the transverse modulus E_{22}. In fact, one of the main motivations of different micromechanics approaches is to give a distinguished expression for the transverse modulus [5]. Tsai and Hahn [47] chose $a_{22} = 0.5$ in a modified rule-of-mixture formula and much better estimations were found for some composites. In light of the fact that $a_{22} = 1$ must be valid when the fiber and the matrix become the same, a formula similar to (B12b) is chosen for a_{22}, i.e.

$$a_{22} = \frac{1}{2}\left(1 + \frac{E^{m}}{E_{22}^{f}}\right), \tag{B20}$$

which corresponds to $\beta_{21} = -0.5$ in (B11b). Finally, using condition (B7), the bridging element a_{44} is found to have the same expression as a_{22}, i.e. Eq. (B20).

By means of the bridging matrix defined above, a set of new formulae for the five engineering moduli of the unidirectional fibrous composite are derived as

$$E_{11} = V_f E_{11}^{f} + V_m E^{m}, \tag{B21}$$

$$\nu_{12} = V_f \nu_{12}^{f} + V_m \nu^{m}, \tag{B22}$$

$$E_{22} = \frac{(V_f + V_m a_{11})(V_f + V_m a_{22})}{(V_f + V_m a_{11})(V_f S_{22}^{f} + a_{22} V_m S_{22}^{m}) + V_f V_m (S_{21}^{m} - S_{21}^{f}) a_{12}}, \tag{B23}$$

$$G_{12} = G^{m}\frac{(G_{12}^{f} + G^{m}) + V_f(G_{12}^{f} - G^{m})}{(G_{12}^{f} + G^{m}) - V_f(G_{12}^{f} - G^{m})}, \tag{B24}$$

$$G_{23} = \frac{0.5(V_f + V_m a_{22})}{V_f(S_{22}^{f} - S_{23}^{f}) + V_m a_{22}(S_{22}^{m} - S_{23}^{m})}. \tag{B25}$$

Eqs. (B21) and (B22) are the rule of mixture formulae for composite longitudinal Young's modulus and Poisson's ratio, which are sufficiently accurate. Eq. (B24) is the result of an exact elastic solution for the overall in-plane shear modulus (G_{12}) of the composite, see Ref. [70]. The accuracy of formula (B23), which is obtained based on Eq. (B20), can be seen from the comparison between predicted and experimental results for the transverse modulus of a glass/epoxy composite shown in Fig. 1 (with $\beta = 0.5$). It is seen that the present model and Chamis's model give comparable results for the transverse modulus of the composite, both of which are in close agreement with the experimental data.

Having validated the correctness and accuracy of the independent bridging matrix elements, Eqs. (B12b), (B18), and (B20), in an elastic region, we can now easily extend them to a plastic region based on a logical consideration. As the bridging matrix correlates the stress states generated in the fiber and matrix materials, it can only depend on the physical and geometrical properties of the constituent materials in the composite. As long as the bridging matrix has been determined using an elastic deformation condition, only the physical properties involved need to be changed when any constituent material undergoes a plastic deformation. The geometrical properties, i.e. the fiber volume fraction, the fiber arrangement in the matrix, the fiber cross-sectional shape, etc. do not change or only vary by a negligibly small amount. Therefore, the independent elements of the bridging matrix should be given by Eqs. (7a)–(7d) (with $\beta = \alpha = 0.5$), whereas the dependent elements of the bridging matrix must be determined by solving Eq. (5). It should be noted that the bridging matrix has the form of Eq. (6) rather than Eq. (B8). This is because the constituent compliance matrix may be fully occupied due to the plastic deformation, see Eq. (15).

Some further remarks deserve mentioning. It has been recognized that the composite longitudinal property (E_{11} together with ν_{12}) is the least "case sensitive". However, the composite transverse and in-plane shear properties are much more dependent on the in situ conditions involved, such as fabrication defects, processing condition, fiber-matrix interface bonding, fiber arrangement, fiber cross-sectional shape. In order to account for these variations, the corresponding independent bridging elements, i.e. a_{22} and a_{66}, may be chosen as variable. This can be achieved

by using, e.g. the following formulae:

$$a_{22} = a_{33} = a_{44} = \beta + (1 - \beta)\frac{E^{\mathrm{m}}}{E_{11}^{\mathrm{f}}}, \qquad 0 \le \beta \le 1, \tag{B26}$$

$$a_{55} = a_{66} = \alpha + (1 - \alpha)\frac{G^{\mathrm{m}}}{G_{12}^{\mathrm{f}}}, \qquad 0 \le \alpha \le 1, \tag{B27}$$

as shown in Eqs. (7b) and (7c). The parameters β and α can be calibrated using measured transverse Young's modulus and in-plane shear modulus, given by Eqs. (11c) and (11d), respectively. It is important to realize that the same parameters α and β can be used in the inelastic and strength analysis of the composite.

References

[1] Chamis CC, Sendeckyj GP. Critique on theories predicting thermoelastic properties of fibrous composites. J Compos Mater 1968;2:332–58.

[2] Hashin Z. Analysis of properties of fiber composites with anisotropic constituents. J Appl Mech 1979;46:453–550.

[3] Hashin Z. Analysis of composite materials — a survey. J Appl Mech 1983;50:481.

[4] Halpin JC. Primer on composite materials analysis. 2nd ed. Lancaster: Technomic, 1992 (p. 153–92).

[5] McCullough RL. Micro-models for Composite materials — continuous fiber composites, micromechanical materials modeling. In: Whitney JM, McCullough RL, editors. Delaware composites design encyclopedia, vol. 2. Lancaster: Technomic, 1990.

[6] Robertson DD, Mall S. Micromechanical analysis and modeling. In: Mall S, Nicholas T, editors. Titanium matrix composites — mechanical behavior, Lancaster: Technomic, 1997. p. 397–463.

[7] Coker D, Ashbaugh NE, Nicholas T. Analysis of the thermomechanical cyclic behavior of unidirectional metal matrix composites. In: Sehitoglu, editor. Thermomechanical fatigue behavior of materials. ASTM STP 1186, 1993. p. 50–69.

[8] Dvorak GJ, Bahei-El-Din YA. Elastic–plastic behavior of fibrous composites. J Mech Phys Solids 1979;27:51–72.

[9] Dvorak GJ, Bahei-El-Din YA. Plasticity analysis of fibrous composites. ASME J Appl Mech 1982;49:327–35.

[10] Hopkins DA, Chamis CC. A unique set of micromechanics equations for high temperature metal matrix composites. NASA TM 87154, First Symposium on Testing Technology of Metal Matrix Composites Sponsored by ASTM, Nashville, 18–20 November 1985.

[11] Chamis CC, Hopkins DA. Thermoviscoplastic nonlinear constitutive relationships for structural analysis of high temperature metal matrix composites. In: Adsit NR, editor. Testing technology of metal matrix composites. ASTM STP 964, Philadelphia, 1988. p. 177–96.

[12] Aboudi J. Micromechanical analysis of composites by the method of cells. Appl Mech Rev 1989;42(7):193–221.

[13] Aboudi J. Micromechanical analysis of composites by the method of cells — update. Appl Mech Rev 1996;49(10):S83–91.

[14] Teply JL, Reddy JN. Unified formulation of micromechanics models of fiber-reinforced composites. In: Dvorak GJ, editor. Inelastic deformation of composite materials, New York: Springer, 1990. p. 341–70.

[15] Brockenbrough JR, Suresh S, Wienecke HA. Deformation of metal-matrix composites with continuous fibers: geometrical effects of fiber distribution and shape. Acta Metal Mater 1991;39(5):735–52.

[16] Huang ZM. A unified micromechanical model for the mechanical properties of two constituent composite materials. Part I: elastic behavior. J Thermoplastic Compos Mater 2000;13(4):252–71.

[17] Huang ZM. A unified micromechanical model for the mechanical properties of two constituent composite materials. Part II: plastic behavior. J Thermoplastic Compos Mater 2000;13(5):344–62.

[18] Huang ZM. A unified micromechanical model for the mechanical properties of two constituent composite materials. Part III: strength behavior. J Thermoplastic Compos Mater 2000 (in press).

[19] Huang ZM. A Unified micromechanical model for the mechanical properties of two constituent composite materials. Part IV: rubber–elastic behavior. J Thermoplastic Compos Mater 2000;13(2):119–39.

[20] Huang ZM. A unified micromechanical model for the mechanical properties of two constituent composite materials. Part V: laminate strength. J Thermoplastic Compos Mater 2000;13(3):190–206.

[21] Huang ZM. Micromechanical prediction of ultimate strength of transversely isotropic fibrous composites. Int J Solids Struct 2000 (in press).

[22] Huang ZM. Tensile strength of fibrous composites at elevated temperature. Mater Sci Technol 2000;16(1):81–94.

[23] Huang ZM. Closed form equations for composite strengths. Submitted for publication.

[24] Huang ZM. Micromechanical strength formulae of unidirectional composites. Mater Lett 1999;40(4):164–9.

[25] Huang ZM. Strength formulae of unidirectional composites including thermal residual stresses. Mater Lett 2000;43(1–2):36–42.

[26] Huang ZM. Effect of matrix plasticity on ultimate strength of composite laminates. J Reinf Plastics Compos 2000 (in press).

[27] Huang ZM. Simulation of inelastic response of multidirectional laminates based on stress failure criteria. Mater Sci Technol 2000;16(6):692–8.

[28] Huang ZM. Modeling strength of multidirectional laminates under thermo-mechanical loads. J Compos Mater 2000 (in press).

[29] Huang ZM. A bridging model prediction of the ultimate strength of composite laminates subjected to biaxial loads. Compos Sci Tech 2000 (in press).

[30] Huang ZM. Micromechanical modeling of fatigue strength of unidirectional fibrous composites. Int J Fatigue 2000 (in press).

[31] Huang ZM. Micromechanical life prediction for composite laminates. Mech Mater 2000 (in press).

[32] Huang ZM. The mechanical properties of composites reinforced with woven and braided fabrics. Compos Sci Technol 2000;60(4):479–98.

[33] Ramakrishna S, Huang ZM, Teoh SH, Tay AAO, Chew CL. Application of leaf and Glaskin's model for estimating the 3D elastic properties of knitted fabric reinforced composites. J Textile Inst, Part 1 2000;91(1):132–50.

[34] Huang ZM, Ramakrishna S, Tay AAO. A micromechanical approach to the tensile strength of a knitted fabric composite. J Compos Mater 1999;33(19):1758–91.

[35] Huang ZM, Ramakrishna S, Tay AAO. Unified micromechanical model for estimating elastic, elasto-plastic, and strength behaviors of knitted fabric reinforced composites. J Reinf Plastics Compos 2000;19(8):642–56.

[36] Huang ZM, Ramakrishna S, Leong KH. Modeling the tensile behavior of Milano rib knit fabric composites. J Reinf Plastics Compos 2000 (in press).

[37] Huang ZM, Ramakrishna S, Tay AAO. Modeling of stress–strain behavior of a knitted fabric reinforced elastomer composite. Compos Sci Technol 2000;60(5):671–91.

[38] Huang ZM, Ramakrishna S, Tay AAO. Micromechanical characterization for the mechanical properties of textile elastomeric composites. Mater Sci Res Int, JSMS 1999;5(3):189–94.

[39] Huang ZM, Ramakrishna S. Micromechanical modeling approaches for the stiffness and strength of knitted fabric composites: a review & comparative study. Composites A 2000;31(5):479–501.

[40] Huang ZM. Towards automatic designing of 2D biaxial woven and braided fabric reinforced composites. Part I: theory. Submitted for publication.

[41] Huang ZM. Towards automatic designing of 2D biaxial woven and

braided fabric reinforced composites. Part II: applications and experimental correlation. Submitted for publication.
[42] Huang ZM. Progressive flexural failure analysis of laminated composites with knitted fabric reinforcement. Submitted for publication.
[43] Huang ZM, Fujihara K, Ramakrishna S. Bending behavior of laminated composites stacked with different angle braids. In: Fifth International Conference on Textile Composites (TexComp-5), Belgium, 18–20 November 2000 (in press).
[44] Adams DF. Elastoplastic behavior of composites. In: Sendeckyj GP, editor. Mechanics of composite materials, New York: Academic Press, 1974. p. 169–208.
[45] Rosen BW, Hashin Z. Effective thermal expansion coefficients and specific heats of composite materials. Int J Engng Sci 1970;8:157–73.
[46] Benveniste Y, Dvorak GJ. On a correspondence between mechanical and thermal effects in two-phase composites. In: Weng GJ, Taya M, Abe H, editors. Micromechanics and inhomogeneity, The Toshio Muta Anniversary Volume. New York: Springer, 1990. p. 65–81.
[47] Tsai SW, Hahn HT. Introduction to composite materials. Lancaster: Technomic, 1980 (p. 377–431).
[48] Chamis CC. Mechanics of composite materials: past, present, and future. J Compos Technol Res 1989;11:3–14.
[49] Berthelot J-M. Composite materials: mechanical behavior and structural analysis. New York: Springer, 1999 (translated by J. Michael Cole, p. 158–81).
[50] Soden PD, Hinton MJ, Kaddour AS. Lamina properties, lay-up configurations and loading conditions for a range of fiber-reinforced composite laminates. Compos Sci Technol 1998;58:1011–22.
[51] Schapery RA. Thermal expansion coefficients of composite materials based on energy principles. J Compos Mater 1968;2:380–404.
[52] Bigelow CA. Thermal residual stresses in a silicon-carbide/titanium [0/90] laminate. ASTM J Compos Technol Res 1993;15:304–10.
[53] Brockenbrough JR, Suresh S. Plastic deformation of continuous fiber-reinforced metal-matrix composites: effects of fiber shape and distribution. Scripta Metall Mater 1990;24:325–30.
[54] Dvorak GJ, Bahei-El-Din, Macheret Y, Liu CH. An experimental study of elastic–plastic behavior of a fibrous boron–aluminum composite. J Mech Phys Solids 1988;36:655–87.
[55] Gates TS, Chen J-L, Sun CT. Micromechanical characterization of nonlinear behavior of advanced polymer matrix composites. In: Deo RB, Saff CR, editors. Composite materials: testing and design, vol. 12. ASTM STP 1274, American Society for Testing and Materials, 1996. p. 295–319.
[56] Hashin Z, Rotem A. A fatigue failure criterion for fiber reinforced materials. J Compos Mater 1973;7:448–64.
[57] Matsuda N, Matsuura K. High temperature deformation and fracture behavior of continuous alumina fiber reinforced aluminium composites with different fiber orientation. Mater Trans, JIM 1997;38:205–14.
[58] ASM Handbook, ASM International. The Materials Information Society, Materials Park, OH 440730002, USA, vol. 6, 1994. p. 992.
[59] Chun HJ, Daniel IM. Behavior of a unidirectional metal-matrix composite under thermomechanical loading. J Engng Mater Technol, ASME 1996;118:310–6.
[60] Awerbuch J, Hahn HT. Off-axis fatigue of graphite/epoxy composite. In: Fatigue of fibrous composite materials, ASTM STP 723. American Society for Testing and Materials, 1981. p. 243–73.
[61] Gibson RF. Principles of composite material mechanics. New York: McGraw-Hill, 1994 (p. 201–7).
[62] Nahas MN. Survey of failure and post-failure theories of laminated fiber-reinforced composites. J Compos Technol Res 1986;8(4):138–53.
[63] Soden PD, Hinton MJ, Kaddour AS. A comparison of the predictive capabilities of current failure theories for composite laminates. Compos Sci Technol 1998;58:1225–54.
[64] Chiu KD. Ultimate strengths of laminated composites. J Compos Mater 1969;3:578–82.
[65] Sendeckyj GP, Richardson MD, Pappas JE. Fracture behavior of Thornel 300/5208 graphite-epoxy laminates — Part 1: unnotched laminates. In: Composite reliability. ASTM STP 580, 1975. p. 528–46.
[66] Robertson DD, Mall S. Incorporating fiber damage in a micromechanical analysis of metal matrix composite laminates. ASTM J Compos Technol Res 1996;18:265–73.
[67] Robertson D, Mall S. Micromechanical analysis and modeling. In: Mall S, Nicholas T, editors. Titanium matrix composites — mechanical behavior, Lancaster: Technomic, 1998. p. 397–464.
[68] Soden PD, Kitching R, Tse PC, Tsavalas Y, Hinton MJ. Influence of winding angle of the strength and deformation of filament-wound composite tubes subjected to uniaxial and biaxial loads. Compos Sci Technol 1993;46:363–78.
[69] Rotem A, Hashin Z. Fatigue failure of angle ply laminates. AIAA J 1976;14(7):868–72.
[70] Hyer MW. Stress analysis of fiber-reinforced composite materials. Boston: McGraw-Hill, 1997 (p. 120–4).